The International Journal of Advanced Manufacturing Technology (2022) 120:7389–7413
https://doi.org/10.1007/s00170-022-09228-7

ORIGINAL ARTICLE

Influence of work-roll grinding error and high-fidelity corrective grinding in cold sheet rolling

Akash Patel[1] · Arif Malik[1] · Feng Zhang[1] · Ritin Mathews[1]

Received: 12 February 2022 / Accepted: 14 April 2022 / Published online: 26 April 2022

Abstract

High-fidelity flatness defects in cold-rolled strip and sheet, arising from highly localized thickness strain variations, present an ongoing challenge to the metal industry. A primary cause of such defects, based on rolling practice, but for which the effects have not been rigorously investigated, is the transfer of localized work-roll diameter deviations due to roll grinding error. This study addresses high-fidelity work-roll diameter deviation transfer in the cold rolling of stainless steel, aluminum, and copper. Parametric studies are performed on a 4-high mill to examine the influences of roll diameter, reduction, strip width, and material on the transfer of high-fidelity work roll diameter deviations. Studies are conducted using an efficient 3D roll-stack model that predicts strip thickness profile deviations via the simplified-mixed finite element method. Reduction deviations on the outgoing strip, which correlate to strip flatness/shape defects, are quantified and analyzed to understand the transfer characteristics of work-roll grinding deviations relative to perfectly ground (smooth) work rolls. The results reveal that high-fidelity transfer depends not only on roll grinding deviation amplitudes and mill loading, but also on the specific locations of deviations along the roll face length due to 3D bulk roll-stack deformations as well as effective stiffness ratio between the work roll and the strip. Concluding the study is a novel approach to identify customized work roll grinding profiles tailored specifically to eliminate pre-existing high-fidelity strip flatness defect patterns, wherein "corrective" high-fidelity roll diameter profiles account for the predicted 3D mill deflections, contact force distributions, and coupled micro-/macro-scale deformation mechanics.

Keywords Cold rolling · Roll diameter deviation · Strip profile/flatness · Roughness/texture transfer · Modeling · In situ corrective roll grinding

Abbreviations

$[\boldsymbol{K_G}]$	Global stiffness matrix
$\boldsymbol{u}$	Global displacement vector
$\boldsymbol{f}$	Global force/load vector
u_j	Translational displacement in x-direction (m)
v_j	Translational displacement in y-direction (m)
w_j	Translational displacement in z-direction (m)
$[\boldsymbol{K_F}]$	Elastic foundation stiffness contribution in the global stiffness matrix
$\left[\boldsymbol{K_T}\right]$	Timoshenko beam stiffness contribution in the global stiffness matrix
k_{f_1}	Elastic foundation stiffness of body 1 at a contact interface (Pa)
k_{f_2}	Elastic foundation stiffness of body 2 at a contact interface (Pa)
$k_{f_{eq}}$	Equivalent elastic foundation stiffness at a contact interface (Pa)
$[\boldsymbol{N}]$	Shape function matrix
l_i	Length of the element i (m)
d_{12}	Distance between the roll center axes for bodies 1 and 2 (m)
x	Location along the width-wise direction (x-direction)
y_c	Initial coordinate (m)
$D(x)$	Diameter profile as a function of location x along the x-direction (m)
δ	Contact interference between two contacting bodies (m)
P_c	Total contact load (N)
E	Young's modulus (Pa)
w	Strip width (m)
H	Entry thickness (m)

✉ Arif Malik
arif.malik@utdallas.edu

[1] The University of Texas at Dallas, 800 W. Campbell Rd, Richardson, TX 75080, USA

h	Exit thickness (m)
F	Rolling force per unit width (N/m)
$\bar{r}$	Average reduction (thickness strain) across the strip width
$\Delta r(x)$	Deviation in thickness strain at location x in the x-direction from the average reduction across the strip width
$\Delta r_{in}(x)$	Deviation in thickness strain at location x in the x-direction from the average reduction across the strip width for the entry strip
$\Delta r_{e}(x)$	Deviation in thickness strain at location x in the x-direction from the average reduction across the strip width for the exit strip
n	Total number of Gaussian points
$\Delta r_{e,e}$	Total reduction deviation of the exit strip considering the errored roll profile
$\Delta r_{e,s}$	Total reduction deviation of the exit strip considering the smooth roll profile
d_{wr}	Diameter of the work roll (m)
l_{wr}	Face length of the work roll (m)
F_{norm}	Normalized specific rolling force
RMS_{lit}	RMS error calculated analogously to the calculations in the literature
RMS_{t}	RMS error calculated per this work using thickness profile
$h(x)_{e}$	Exit thickness profile as a function of axial location x considering the grinding error on the work roll (m)
$h(x)_{u}$	Exit thickness profile as a function of axial location x considering the smooth profile of the work roll (m

1 Introduction

The dimensional quality of cold rolled strip and sheet is extremely critical to downstream manufacturing operations, which is why it continues to be a primary area of research (Fig. 1). Deviations from the desired thickness profile and flatness of the strip arise due to localized variations in the relative plastic deformation (i.e., thickness reduction) across the strip width, which subsequently produce widthwise or transverse variations in the longitudinal residual stress in the strip. Accordingly, for decades, efforts have focused on achieving uniform transverse distribution of longitudinal stresses by abating or controlling widthwise deviations in the plastic thickness strain (or relative thickness reduction). The cause of such deviations is largely attributed to mismatch between the loaded roll gap profile and the incoming strip thickness profile. While many factors contribute to the loaded roll gap profile, among the most influential are (1) roll-stack deformation involving bending, shearing, and Hertzian flattening of rolls (Fig. 1b); (2) transient roll diameter variations, as exemplified by the "warm" and "cold" (and worn) work roll diameter profiles in Fig. 1c; and (3) the imperfect grinding of new rolls based on residual error from the grinding process (e.g., "new" roll diameter profile in Fig. 1c). The dimensional quality of rolled strip, as influenced by the foregoing factors, is broadly addressed in terms of thickness profile and flatness (or shape), although the two are interdependent due to mass conservation. In the cold rolling of thin metals in particular, widthwise expansion of strip or sheet is negligible. Thus, from conservation of mass during plastic deformation, transverse perturbations in the relative thickness reduction induce corresponding localized regions of lengthwise expansion or contraction, which subsequently result in localized negative and positive longitudinal residual stress regions, respectively [2]. When free of applied rolling tensions, these residual stresses can manifest as visibly tight or loose (i.e., buckled) flatness defects (see Fig. 1d). With the heightened sensitivity of flatness to changes in the roll gap profile for thin materials, control of the thickness profile itself is usually impractical and is undertaken only to achieve desired flatness. Evolution of rolling technology to meet the demands of increased strip quality has led to flatness control devices such as roll bending, machined roll profiles such as parabolically crowned rolls or more advanced continuously variable crown (CVC) roll profiles integrated with axial roll shifting, as well as thermal control of roll profiles.

While these control mechanisms address typical low-to-medium fidelity flatness defects (see Fig. 2), the correction of localized and complex higher order defects, as seen in Fig. 1d, has not seen much success and thus frequently necessitates post-process operations such as tension or roller leveling. Such high-fidelity flatness defects can result from abrupt transverse changes along the loaded roll gap profile, resulting, for example, from the localized work roll diameter variations shown in Fig. 1c according to operational state of the roll. Since the strip is softer than the work roll, such local diameter deviations can partially transfer to the strip [3], potentially adversely affecting flatness via such defects as shown in Fig. 1d.

Although conventional flatness control mechanisms cannot easily correct high-fidelity defects, thermal roll profile control offers some benefit since a typical spray header cooling system comprises of series of nozzles capable of independent actuation with different coolant temperatures to change the effective diameter or lubrication over narrow zones along the roll face [4]. However, the continuous state of heat transfer, which leads to thermal interference in neighboring zones, together with non-uniform heat generation along the roll/strip interface, results in a complex thermal scenario which in itself has been an area of research for many years and limits effectiveness of spray header control systems. In addition, the width of the area/zone for each nozzle typically

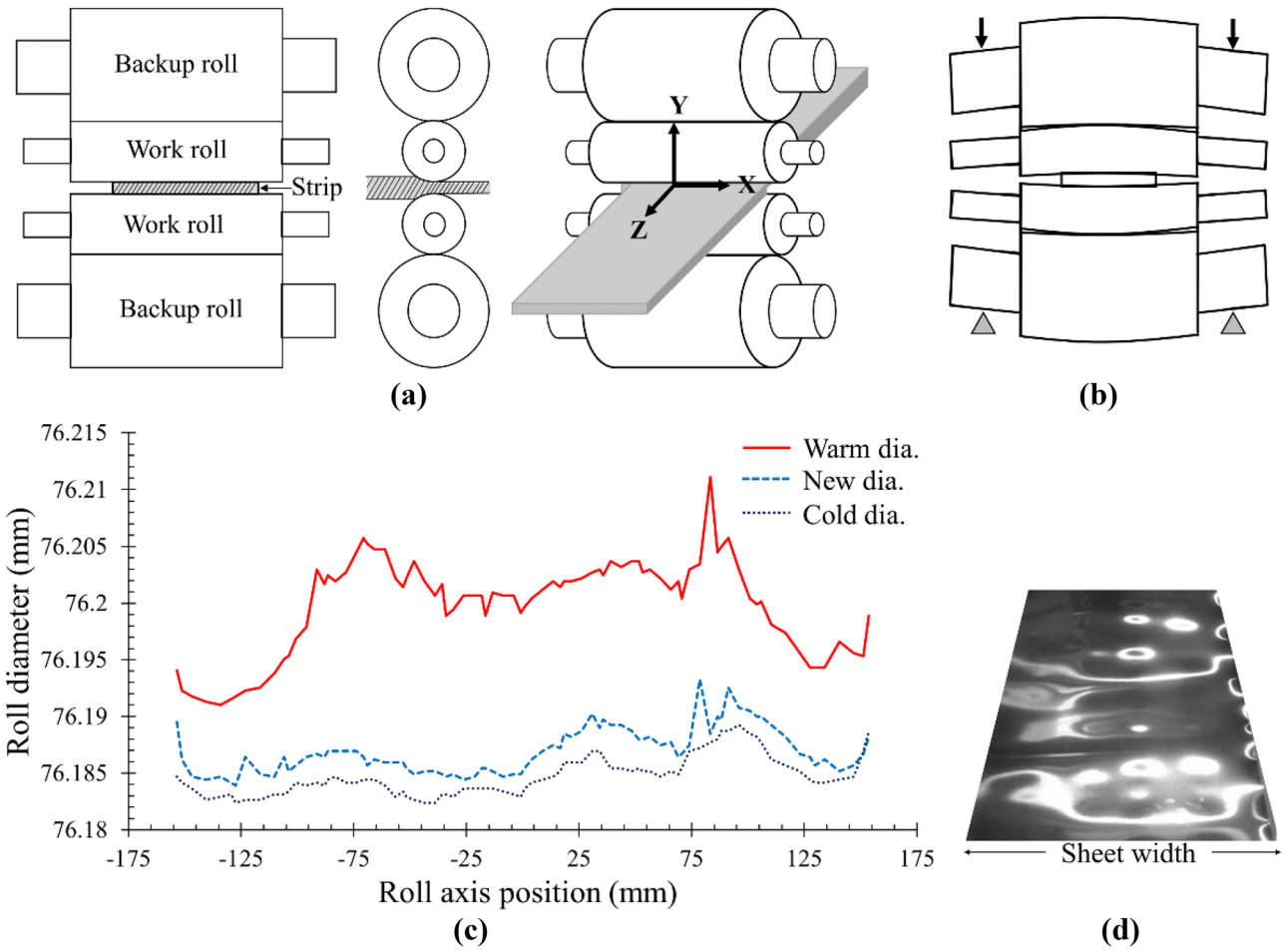

Fig. 1 **a** 4-high rolling mill stand; **b** exaggerated natural mill deflection behavior of 4-high mill stand, involving bending, shear, and flattening of rolls; **c** measured roll diameter profiles for a new work roll, the same roll when warm (after a single old rolling pass), and the same roll when cold and worn (after multiple passes); **d** section of a thin strip showing complex flatness (shape) defects [1]

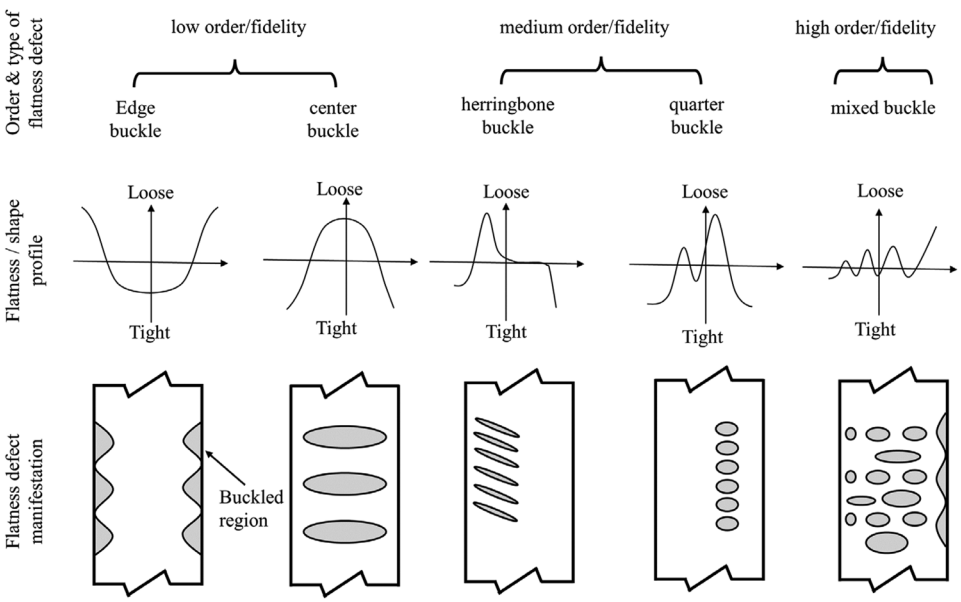

Fig. 2 Order and types of flatness/shape defects in cold rolled strip/sheet

ranges from 25 to 100 mm [4], which may be insufficient to remove highly localized defects. Moreover, spray header thermal control systems apply only to 2-high, 4-high, and 6-high mill configurations, but not to 20-high cluster mills where lubricant "floods" the roll-bite, and for which high-quality rolling of high-strength, thin strip can be critical.

Since the implementation of any new type of flatness control mechanism designed to correct for high-fidelity defects will benefit from a detailed understanding of the transfer characteristics from the work roll to the strip, this paper provides both a rigorous modeling approach and parametric case studies toward this goal. Investigated in the parametric studies are transfer characteristics of high-fidelity work roll diameter deviations (e.g., Fig. 1c) onto the strip profile as a function of reduction ratio, roll diameter, and strip width considering three materials of differing strength (301 stainless steel, 6061-O aluminum, and commercially pure copper). Also investigated in this paper is a novel and potentially effective means to design corrective high-fidelity work roll diameter profiles tailored to incoming high-fidelity strip profile defects and adjusted according to the predicted mill and strip contact deformation mechanics. Upon commissioning of an appropriate in situ grinding and debris removal system, it might one day be possible to implement such "corrective" roll grinding profiles in situ during rolling (or between passes) to much more effectively eliminate high-fidelity flatness defects.

Note that while the above discussion is in the context of dimensional quality under an assumption of quasi-static conditions, dimensional quality can also be affected by the dynamics of the rolling process, which results directly or indirectly in transient variations in the roll gap spacing and thus the exit strip gauge. At or above particular rolling speeds, the interactions between the rolling process dynamics and the mill structural dynamics can lead to dynamic instability and cause "chatter" vibrations, which adversely affect the dimensional quality. Such investigations require a coupled modeling approach between a structural dynamics model (as summarized in [1]) and a rolling process dynamics model (e.g., [5–9]) to capture the respective behaviors. Ongoing efforts have been made to identify conditions of instability that lead to chatter vibrations [5, 6, 9–15]; however, for the objectives of the current investigation, a static model is sufficient.

While published work directly related to the 3D transfer of high-fidelity work roll diameter deviations to the rolled strip is absent, the literature on roughness and texture transfer is closely related and is discussed next in Sect. 1.1. Following this, Sect. 1.2 provides details of the 3D roll-stack model for predicting high-fidelity strip thickness profile deviations using the simplified-mixed finite element method (SM-FEM). Section 2 applies the model in the.parametric case studies of the transfer characteristics. Section 3 illustrates the inability of common work roll bending systems to correct for high-fidelity defects. Section 4 demonstrates the design and performance of customized corrective roll grinding profiles, and Sect. 5 offers concluding remarks regarding potential implementation of such a system.

1.1 Review of related studies on roughness/texture transfer

Texture/roughness transfer is a closely related phenomenon to the transfer of high-fidelity roll diameter deviations. Texture transfer is characterized by two underlying mechanisms: penetration of work roll texture into the strip (dominant in low elongations/reductions) and reverse extrusion (where strip material flows into roll valleys), which is predominant in large reductions [31]. While texture/roughness transfer is fundamentally distinct from roll diameter deviation transfer, the similarity in their mechanism justifies a review of texture/roughness parametric transfer effects. Such effects in the cold rolling process occur not only at the macroscopic scale but also at very small scales of about 50 nm [32]. Physics-based modeling of such complex phenomena, which involves highly nonlinear elastic–plastic macro-scale roll bite mechanics as well as surface asperity contact mechanics, presents significant challenges. Accordingly, computational research in this area relies heavily on simplifying assumptions for continuum finite element simulations or other analysis methods. In addition, most experimental studies use simplified laboratory-scale mills. Table 1 summarizes observations and conclusions from the corresponding texture/roughness transfer investigations to date.

As indicated in Table 1, computational efforts to understand and characterize the transfer behavior of surface roughness predominantly involve 2D plane strain analyses (e.g., [21, 22]). Recent work, however, shows that these 2D models neglect significant coupling effects between the micro-scale asperity contact mechanics and the macro-scale 3D bulk body deformations (bending, shear, and Hertzian flattening) of the mill components [33]. Furthermore, all but two experimental studies in Table 1 apply laboratory mills, which typically do not replicate the deformation and load characteristics of production mills. Notwithstanding their value in understanding roughness effects, a drawback of the experimental observations is that correlations between the effects of multiple variables make it impractical to infer and understand the isolated effects of specific variables in a parametric assessment. Despite this, the roughness/texture literature in Table 1 provides important related observations that will be discussed and compared to the results in this work.

It should be noted at this point that the fundamental distinction between high-fidelity roll diameter deviations (from residual grinding error) and roll roughness is that the latter is characterized as high-frequency, short-wavelength variations from an ideal surface, whereas the high-fidelity

Table 1 Observations from related texture/roughness transfer literature

Author(s) (year)	Method	Material	Investigation	Observations/conclusions
Özakın et al. [16]	Experimental	DC04 steel	Effect of thickness change and reduction ratio	Roughness transfer is higher in higher reduction ratios Higher roughness transfer in thinner sheet at lower roughness values while in thicker sheet with higher roughness values
Wu et al. [3, 17]	2D plane strain analytical slab method; finite element analysis (FEA)	Material with specified properties	Non-steady state roughness prediction modeling	Roughness transfer increases with an increase in reduction ratio but reaches a plateau
Çolak et al. [18]	Experimental	DC01 carbon steel	Effects of rolling parameters on roughness transfer in temper rolling	Roughness transfer increases with an increase in rolling speed Roughness transfer increases with an increase in rolling force Greater transfer is expected in thinner materials
Xia et al. [19]	Statistical analysis of industrial strip data	Steel	Prediction model based on degree of influence of different parameters	Most influential factor on the roughness is the product of reduction and tension ratios
Wentink et al. [20]	Experimental	Annealed, hot dip, galvanized interstitial free steel	Model for roll roughness, roll wear and roughness transfer	Roughness of the strip increases with an increase in rolling force Roughness of the strip increases with an increase in reduction ratio Roll surface is mirrored onto strip
Kijima [21, 22]	2D plane strain FEA; 2D plane strain Experiments	Annealed low carbon steel	Influence of roll radius on roughness transfer in temper rolling	For the same peak pressure, roughness transfer ratio is higher with smaller roll
Li et al. [23]	Experimental	SUS430 Stainless steel	Relation of roughness and glossiness	Average roughness (Ra), maximum height of peak, and valley decreases with an increase in reduction ratio
Belov et al. [24]	Experimental; strip data analysis	Steel	Effects of reduction, thickness, roll diameter, and tensile stress on roughness transfer	Roughness of the strip increases with an increase in reduction to exit thickness ratio Roughness of the strip increases with an increase in strength of the strip material Roughness of the strip increases with an increase in roll diameter Roughness of the strip increases with an increase in tensile stress on strip in the deformation region
Kimura et al. [25]	Experimental	galvanized steel	Investigation of texture transfer in galvanized steel	Roughness transfer increases with an increase in elongation (reduction) Roughness transfer increases with an increase in roll diameter

Table 1 (continued)

Author(s) (year)	Method	Material	Investigation	Observations/conclusions
Kijima & Bay [26, 27]	2D plane strain FE analysis; 2D plane strain Experiments	Annealed low carbon steel	Influence of tool roughness in temper rolling on roughness transfer and strip elongation	Shear stress caused by tangential displacements have significant effect on the amount of roughness transfer Roughness transfer is dominated by peak pressure
Tieu et al. [28]	Experimental	Carbon steel and aluminum alloy	Relationship of friction coefficient and process parameters	Roughness of the strip increases with an increase in reduction ratio Rolling force increases with higher surface roughness of the strip
Ma et al. [29]	Experimental	Carbon steel	Analysis of reduction ratio, speed by atomic force microscope analysis of strip surface	Roughness of the strip increases with an increase in rolling speed Roughness of the strip increases with an increase in reduction
Le et al. [30]	Industry strip analysis	Aluminum alloy	Spectral analysis of the industry rolled strip surface	Strip surface nearly conforms to the work roll surface in the initial pass Long wavelength components flatten more rapidly than short wavelength components on the strip surface

deviations are considered dimensional irregularities from an ideal geometry (characterized by relatively similar scale amplitude as roughness but much larger wavelength). Perhaps the most important aspect that differentiates high-fidelity roll diameter deviations from roll surface roughness is their respective behaviors; from a contact mechanics viewpoint, roughness behaves mechanically different from the rest of the body underneath and can initially be considered as a reduced strength layer, while the high-fidelity deviations exhibit mechanical deformation behavior similar to that the bulk body, and thus they more substantially influence bulk deformation behavior. It is therefore necessary to understand the transfer behavior of high-fidelity deviations in the context of a 3D roll-stack contact mechanics environment, which includes examining coupling effects between the bulk-body deformation and the roll diameter deviations under parametrically varied rolling conditions. Accordingly, provided next is a mathematical description of the 3D roll-stack modeling approach used to predict strip thickness profile deviations for the parametric studies, as well as the subsequent corrective roll grinding investigation.

1.2 Strip profile prediction mathematical formulation

Model formulations developed over the years to predict steady-state strip thickness profile have incorporated methods based on influence coefficients, transport matrices, large-scale continuum finite element analyses, and non-physics pattern recognition techniques, as summarized in [35–37]. On account of applicability to complex mill configurations (e.g., 20-high cluster mills [38]), as well as computational cost and accuracy requirements, the physics-based simplified mixed finite element method (SM-FEM), introduced in [35] and adapted with an advanced contact algorithm to accommodate both low order and high-fidelity roll profiles [33, 34, 39, 40], is adopted herein. Although the SM-FEM model described can be coupled with a Newmark-beta time integration technique to simulate temporal behavior of the 3D roll-stack and predict transient evolution of the rolled strip profile (as described in [1]), a static model is sufficient for the investigations in this work.

The detailed model validation and derivation, including use of coupled Winkler foundation elements, 3D Timoshenko beam elements, calculation of contact interferences, and the overall procedure for assembly and solution of the nonlinear system of equations is given in previous work [33, 39]. Hence, only outlined in this section is the formulation necessary for implementation, as well as a comparison of results to large-scale continuum FEM.

Figure 3a provides a schematic of the SM-FEM formulation. Bending and shear deformations of rolls are

modeled using 3D Timoshenko beam elements. Nonlinear elastic contact flattening due to Hertzian behavior per the analytical expression in [41], as well as the equivalent load versus plastic deformation relation of the strip, is modeled using the twin beam-coupled Winker foundation elements. This formulation avoids the requirement for a large number of very small elements to represent the narrow contact regions, as is the case with conventional continuum FEM.

Equation (1) represents the corresponding global nonlinear system of equations, where the global stiffness matrix, $[\boldsymbol{K_G}]$, and load vector, $\boldsymbol{f}$, are functions of the displacement vector, $\boldsymbol{u}$ [35]

$$\left[\boldsymbol{K_G}(\boldsymbol{u})\right]\boldsymbol{u} = \boldsymbol{f}(\boldsymbol{u}) \tag{1}$$

Each displacement vector, u_j, at node j includes three translation and three rotation degrees of freedom:

$$\boldsymbol{u}_j = \left\{u_j v_j w_j \theta_{xj} \theta_{yj} \theta_{zj}\right\} \tag{2}$$

The global stiffness matrix, $[\boldsymbol{K_G}]$, in Eq. (1) is superposed by a Winkler continuous nonlinear foundation stiffness matrix contribution, $[\boldsymbol{K_F}]$, and the standard Timoshenko matrix contribution for bending and shear deformable stiffness, $[\boldsymbol{K_T}]$, per Eq. (3):

$$\left[\boldsymbol{K_G}\right] = \left[\boldsymbol{K_F}\right] + \left[\boldsymbol{K_T}\right] \tag{3}$$

For a coupled beam/foundation element i between bodies 1 and 2, respectively (e.g., strip and work roll as in Fig. 3a, or two rolls), the total coupled element stiffness, $\left[\boldsymbol{K_G}^{1,2,i}\right]$, has a size 24 by 24 and contains all six translational and rotational degrees of freedom at each of the four nodes (see two Timoshenko beam elements coupled with intervening foundation in Fig. 3), as in Eq. (4):

$$\begin{aligned}\left[\boldsymbol{K_G}^{1,2,i}\right] &= \left[\boldsymbol{K_F}^{1,2,i}\right] + \left[\boldsymbol{K_T}^{1,2,i}\right] \\ &= \begin{bmatrix} \int_0^{l_i} k_{feq}(x)\left[\boldsymbol{N}_{11}\right]dx & -\int_0^{l_i} k_{feq}(x)\left[\boldsymbol{N}_{12}\right]dx \\ -\int_0^{l_i} k_{feq}(x)\left[\boldsymbol{N}_{21}\right]dx & \int_0^{l_i} k_{feq}(x)\left[\boldsymbol{N}_{22}\right]dx \end{bmatrix} \\ &+ \begin{bmatrix} \left[\boldsymbol{K_T}^{1,i}\right] & [0] \\ [0] & \left[\boldsymbol{K_T}^{2,i}\right] \end{bmatrix}\end{aligned} \tag{4}$$

In Eq. (4), l_i is the i^{th} element length. For bodies 1 and 2, the shape function matrix subset term $\left[\boldsymbol{N}_{\surd\text{II}}\right]$ (for $\surd, \text{II} \in [1,2]$) in the foundation stiffness matrix $\left[\boldsymbol{K_F}^{1,2,i}\right]$ is defined as:

$$\begin{aligned}\left[\boldsymbol{N}_{\surd\text{II}}\right] &= \left[\left[\boldsymbol{N}_{v\text{II}}\right]^T\left[\boldsymbol{N}_{v\text{II}}\right]\sin^2\theta + \left[\boldsymbol{N}_{w\surd}\right]^T\left[\boldsymbol{N}_{w\text{II}}\right]\cos^2\theta\right. \\ &\left. + \left[\boldsymbol{N}_{v\surd}\right]^T\left[\boldsymbol{N}_{w\text{II}}\right]\sin\theta\cos\theta + \left[\boldsymbol{N}_{w\surd}\right]^T\left[\boldsymbol{N}_{v\text{II}}\right]\sin\theta\cos\theta\right]\end{aligned} \tag{5}$$

where $[\boldsymbol{N}]$ represents the full shape function representing both horizontal (w) and vertical (v) displacements of conventional Timoshenko beams. Term θ in Eq. (5) is the angle of inclination between bodies 1 and 2, where, for example, $\theta = 90°$ corresponds to a vertically oriented 4-high mill as shown Fig. 1. Matrix $\left[\boldsymbol{K_T}^{1,2,i}\right]$ in Eq. (4) is size 24×24 and contains the 12×12 element stiffness matrices, $\left[\boldsymbol{K_T}^{1,i}\right]$ and $\left[\boldsymbol{K_T}^{2,i}\right]$, for 3D Timoshenko beams 1 and beam 2, respectively.

Iterative techniques for the solution of nonlinear static system in Eq. (1) are discussed in [28], although at a given mill operating condition such as during the same rolling pass, $[\boldsymbol{K_G}]$ can be considered constant [35], thus linearizing the system in Eq. (1).

1.2.1 Contact interference

In an elastic contact model between rolls, the distance, d_{12} between roll center axes 1 and 2, is computed from the relative displacement $v_1(x) - v_2(x)$ and initial coordinates, y_c.

$$d_{12} = \left[y_{1c} + v_1(x)\right] - \left[y_{2c} + v_2(x)\right] \tag{6}$$

For estimation of the contact interference, δ_{12}, a distance function between the axes is applied (using respective local diameter), as expressed in Eq. (7) [35]

$$\delta_{12}(x) = D_1(x) + D_2(x) - d_{12}(x) \tag{7}$$

The roll diameter profile deviations are incorporated into $D_1(x)$ and $D_2(x)$ for the contact interference calculation. The specific contact force $f(x)$ is the product of the contact interference and the equivalent foundation stiffness, $kf_{eq}(x)$, which is derived from the series stiffness combination between the elastic foundation stiffness of bodies 1 and 2 (strip/roll or roll/roll). The integral of the specific contact force requires equilibration with the total applied contact load, P_C.

$$\begin{aligned}P_C &= \int_0^l f(x)dx = \int_0^l kf_{eq}(x)\delta_{12}(x)dx \\ &= \int_0^l \left(\frac{1}{kf_1(x)} + \frac{1}{kf_2(x)}\right)^{-1}\delta_{12}(x)dx\end{aligned} \tag{8}$$

The SM-FEM model described above has been validated against both large-scale finite element models as well as industrial data involving asymmetric roll profiles such as CVC [40]. A detailed comparison of SM-FEM with large scale finite element analysis to investigate the capability of the SM-FEM to capture high-fidelity roll diameter deviations and contact force perturbations was carried out in [34] and shows strong agreements in the results (Fig. 3b). The model not only provides an effective and efficient method to predict the steady-state strip profiles under high-fidelity

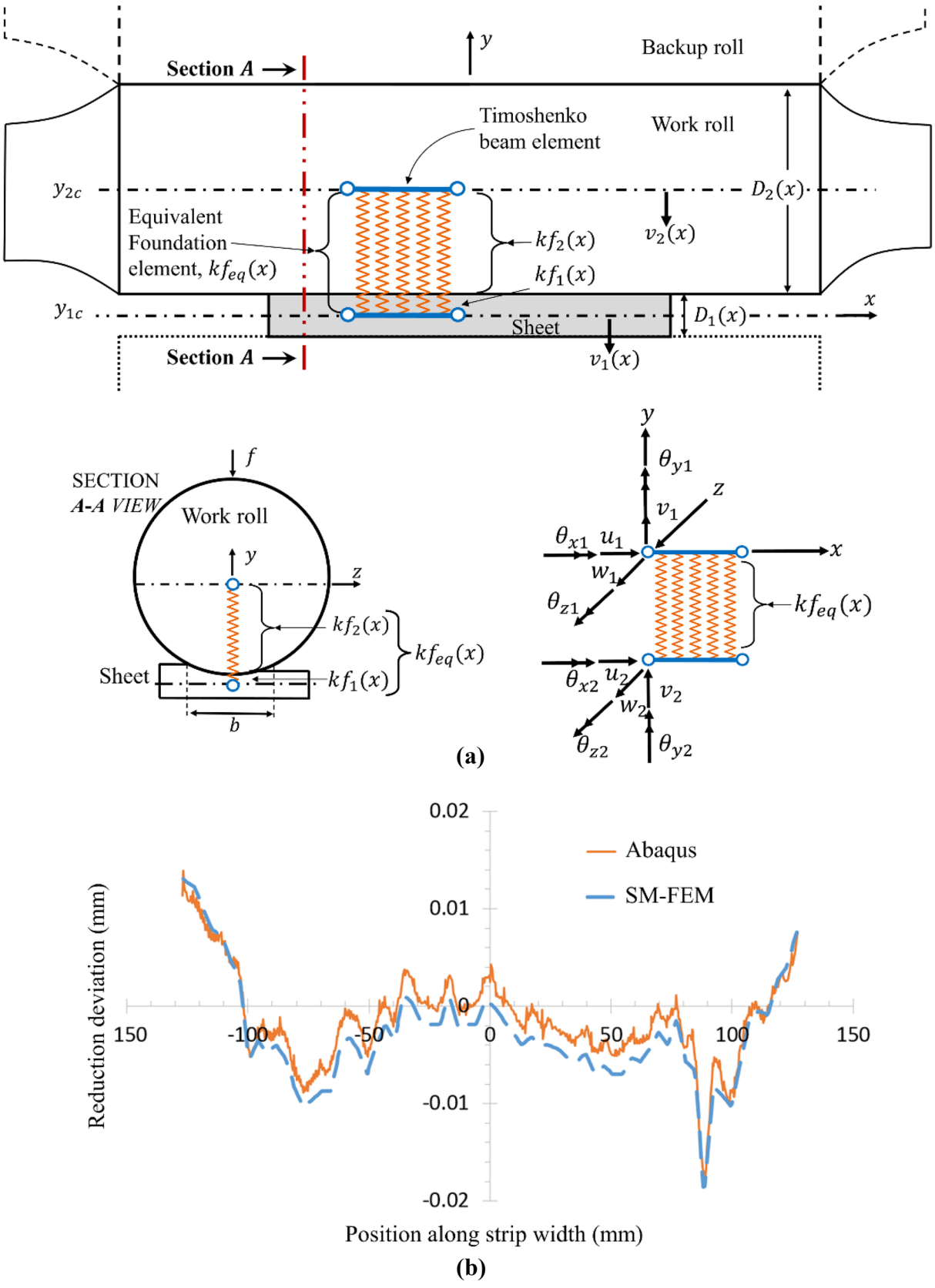

Fig. 3 **a** Mixed continuous Winkler elastic foundation and 3D Timoshenko beam element with nodal degrees of freedom between adjacent bodies 1 and 2; **b** reduction deviation comparison between SM-FEM and large-scale continuum finite element analysis using Abaqus [34]

conditions, but being 3D, the roll-stack model proves to be superior over the simplified 2D plane-strain models by capturing the coupling between the contact mechanics and bulk body deformation.

To estimate rolling force for the three different materials (301 stainless steel, 6061-O aluminum, and commercially pure copper), the simple mathematical model by Roberts, explained in [42], is adopted here. Note that although more sophisticated roll-bite force models are available, the aim here is simply to incorporate rolling force trends for the three materials in parametric studies involving high-fidelity transfer using the aforementioned 3D roll-stack deformation model.

2 High-fidelity transfer

Investigated in this section are the transfer characteristics of high-fidelity work roll diameter deviations (grinding error) represented by the "warm" profile of Fig. 1c. Case studies are carried out for a 4-high cold rolling mill stand model (Fig. 1a) to investigate the individual influences of (i) nominal work roll diameter, (ii) strip width, and (iii) reduction ratio for each of the three material types. For better understanding of the parametric effects, only the upper work roll incorporates high fidelity roll grinding deviations, while all other rolls (including the bottom work roll) are considered to be perfectly smooth. The incoming strip also assumes a perfectly smooth incoming state and has rectangular thickness profile (i.e., no incoming crown). In addition, the influences of nominal work roll diameter, strip width, and reduction on the high-fidelity transfer characteristics are investigated using two different nominal incoming thickness categories: (i) 2.576 mm initial strip having no prior reduction since anneal (referred to hereinafter as "thick gauge") and (ii) 0.236 mm final-pass, significantly work-hardened strip having 41.875% prior reduction (with isotopic strain hardening according to Ludwik's power law, referred to hereinafter as "thin gauge"). Again, each parametric case includes the three material types: SS 301 as high strength material, Al 6061-O with 90 min aging for medium strength, and commercially pure copper (Cu) as soft material.

Nominal/reference rolling pass cases for both the thick and thin gauge strips are first defined to serve as benchmarks for the parametric comparisons. Table 2 lists the associated mill dimensions and nominal case parameters. Material constitutive parameters used with Ludwik's isotropic strain hardening for subsequent rolling force estimations are tabulated in Table 3. Entry to exit tension ratio is 0.734 with entry tension kept at 11% of the yield strength of the material. With the "warm" work roll diameter profile from Fig. 1c (referred to hereinafter as "errored" roll profile) applied to the upper work roll, a mesh convergence study for the described SM-FEM method was first carried out to achieve convergence in the average strip thickness strain and to ensure effective capture of the high-fidelity deviations. A total of 224 foundation-coupled, double Timoshenko beam elements (see Fig. 3a lower right) were found to be sufficient for all case studies.

Table 2 Mill dimensions and nominal case parameters

Parameter	Value
Work roll diameter	76.2 mm
Backup roll diameter	304.8 mm
Work roll face length	304.8 mm
Backup roll face length	304.8 mm
Work roll neck diameter	50.8 mm
Backup roll neck diameter	187.2 mm
Work roll neck length	152.4 mm
Backup roll neck length	152.4 mm
Distance between bearings on work roll	457.2 mm
Distance between bearings on backup roll	457.2 mm
Work roll and backup roll Young's modulus	207 GPa
Strip width (nominal case)	209.55 mm
Entry thickness (for thick gauge nominal case)	2.576 mm
Exit thickness (for thick gauge nominal case)	2.382 mm
Reduction ratio (for thick gauge nominal case)	7.495%
Entry thickness (for thin gauge nominal case)	0.236 mm
Exit thickness (for thin gauge nominal case)	0.234 mm
Reduction ratio (for thin gauge nominal case)	1.075%

Table 3 Material constitutive model parameters for Ludwik's isotropic hardening used to estimate specific rolling force

Material	Yield strength (MPa)	Strength coefficient (MPa)	Strain hardening exponent
SS 301	283.37	2987.49	0.7475
Al 6061-O	118.87	356.99	0.21
Cu	69	530	0.44

Table 4 Estimated normalized specific rolling force for nominal cases

Material	Normalized force ($\frac{P_c}{Ew} \times 10^4$)	
	Thick gauge	Thin gauge
SS 301	0.45	0.60
Al6061-O	0.22	0.05
Cu	0.15	0.05

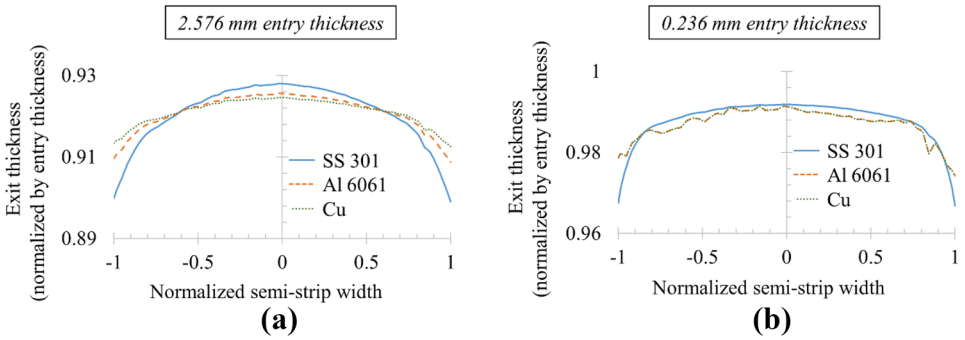

Fig. 4 Exit thickness profile of nominal cases in Table 2. **a** Thick gauge (2.567 mm); **b** thin gauge (0.236 mm)

2.1 High-fidelity roll grinding error transfer characteristics for nominal cases

Table 4 lists the required rolling force per unit strip width (normalized to work roll elastic modulus) for the thick and thin gauge nominal rolling cases in Table 2. Figure 4 shows the resulting exit thickness profiles normalized by input thickness for both the thick gauge (Fig. 4a) and thin gauge (Fig. 4b) nominal cases considering the three material types, and when rolled using an upper work roll containing the warm residual grinding error from Fig. 1c.

In Fig. 4, transferred high-fidelity deviations are clearly visible on all but one of the exit thickness profiles as a direct result of the work roll grinding error. Also, even though all three materials are simulated with identical mill parameters, the relative contact forces and distributions vary between SS 301, Al 6061-O, and Cu due to the respective material strengths, which results in different thickness profiles. The 301 stainless steel strip, possessing the highest strength, induces greater bending and edge-flattening of the rolls, leading to greater "natural" strip crown compared to the Al 6061 and Cu.

Regarding the high-fidelity roll grinding error transfer, it is intuitive that the extent of deviations transferred to the strip depends on a number of variables such as elastic stiffness of work rolls, elastic stiffness, and plastic resistance of strip, as well as bulk body deformations such as bending, shear, and variation in Hertzian flattening along the roll face lengths. A combination of these effects, accounted for by the SM-FEM model, determines the actual contact force distribution at the roll/strip interface and governs the degree of transfer of work roll geometrical deviations onto the strip. These combined effects are manifested in Fig. 4 as differences in transfer among the three materials at any given location along the strip width. For the thin gauge, however, the exit profiles for Al 6061 and Cu appear to overlap; this is due similarity in the strain-hardened material strengths (405 MPa for the Al 6061 and 401 MPa for Cu), as well as their similar required specific rolling forces with 41.875% prior reduction (see Table 4). To better visualize the transfer effects of the work roll grinding error, Fig. 5a, b reveals the differences in exit thickness profiles relative to the case in which high-fidelity grinding error is absent (i.e., relative to a perfectly smooth upper work roll). Considering first Fig. 5a, the results shown help reveal the transfer characteristics by eliminating the influences of bulk body deformation.[1] This is because at any transverse distance from mill center, the exit thickness profiles in the earlier Fig. 4a arise due to combination of effects that include bending, shear, and non-uniform flattening of the rolls, yet these innate effects (which are similar but not identical for the errored roll and the smooth roll [43]) are now eliminated, as is evident in Fig. 5a. Despite the different individual shapes of the exit thickness profiles among the three materials in Fig. 4a, the profiles seen in Fig. 5a, by "filtering" the bulk-body deformation, are in fact very similar and clearly exhibit noticeable transfers of the roll grinding error. In the case of SS 301, the thick-gauge error transfer shown in Fig. 5a is comparable with that of Al 6061 and Cu; however, for thin gauge (Fig. 5b), the error transfer for SS 301 is almost negligible compared to Al 6061 and Cu; because of the more significant work-hardening and higher strength of SS 301, the thin gauge strip experiences less transfer.

This can be explained by analyzing the relative "stiffnesses" of roll and strip during plastic deformation as follows. Defined in Eq. (9) is the average foundation stiffness modulus of the strip, kf_1, used in the SM-FEM model described earlier, where F is the total rolling force, w is the strip width, and $(H-h)$ represents the absolute reduction. At the mill operating point, the strip modulus kf_1 represents the secant[2] (Fig. 5e) (or tangent) of unit rolling force versus plastic thickness reduction:

$$kf_1 = \frac{F}{w(H-h)} \tag{9}$$

[1] Ref. [23] showed the coupling effects between micro- and macro-scale deformation.

[2] Secant is preferred over tangent particularly in dynamic analysis with direct time integration.

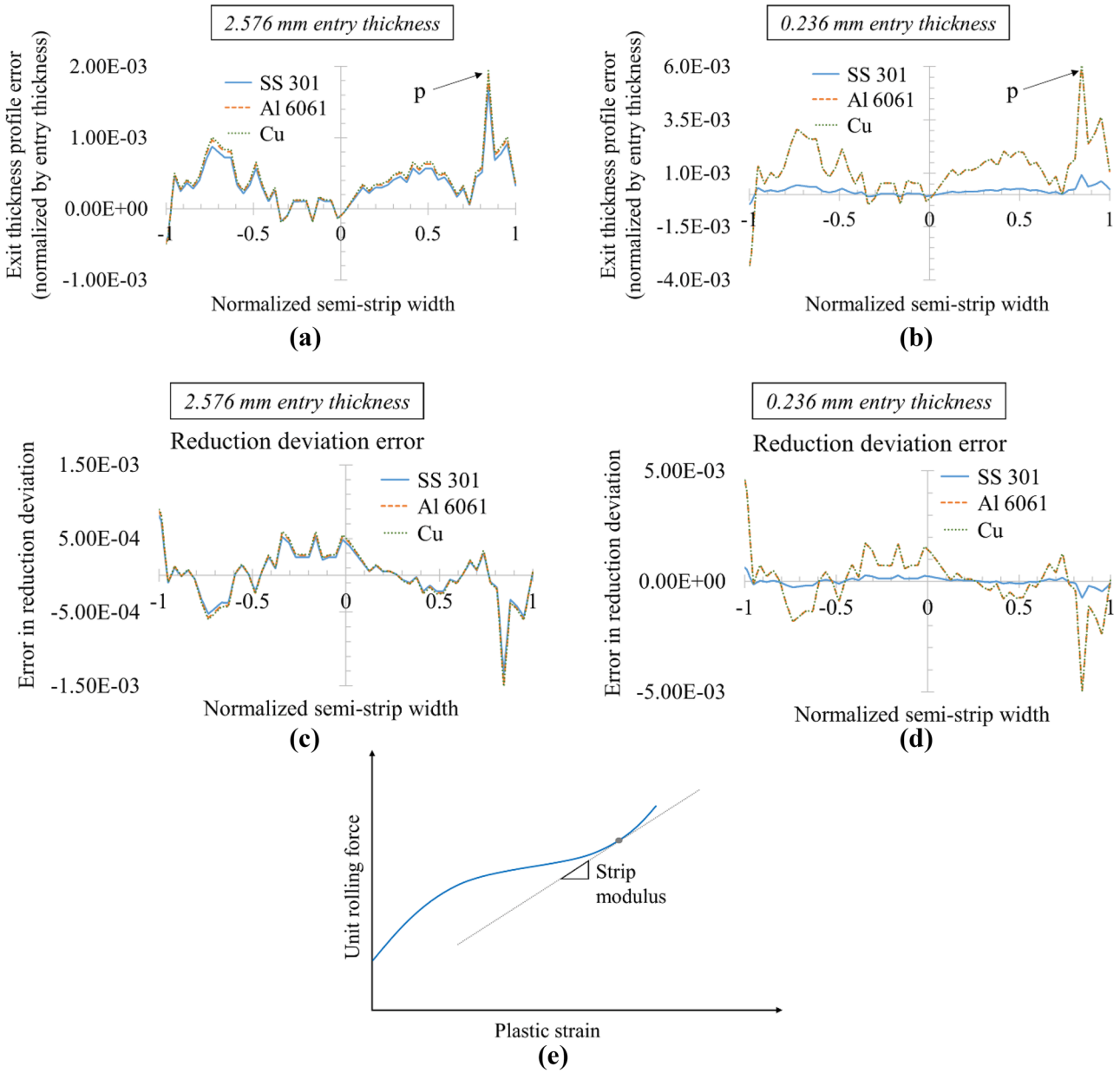

Fig. 5 Thickness profile deviation/error of strip in errored roll relative to smooth roll case for **a** thick gauge (2.567 mm); **b** thin gauge (0.236 mm); **c** and **d** corresponding error in reduction deviation; **e** constant linearized strip foundation modulus

$$kf_{eq} = \left[kf_1{}^{-1} + kf_2{}^{-1}\right]^{-1} \tag{10}$$

Equation (10) defines the corresponding total equivalent foundation stiffness between the work roll axis and the strip horizontal mid-plane, where kf_2 is the elastic flattening stiffness of the work roll.

Listed in Table 5 are the average values of the strip modulus kf_1, the work roll foundation flattening modulus kf_2, and the combined equivalent elastic foundation stiffness, kf_{eq}, for the nominal thick and thin gauge cases for all three materials. Note that the high-fidelity transfer mechanics from the work roll to the strip are directly related to the ratio between kf_1 and kf_2, values for which are also given. In the case of SS 301, the kf_1/kf_2 ratio increases by factor of 100 from the thick to the gauge, which explains the insignificant transfer of roll deviations. In contrast, for the softer Al 6061 and Cu materials, this ratio for thick and thin gauge differs by only one order of magnitude. Even though kf_1/kf_2 is comparatively larger both for the thin gauge Al 6061 and Cu than it is for thick gauge, the ratio is still relatively small,

Table 5 Average values of foundation stiffnesses kf_1,kf_2,and kf_{eq}, as well as the ratio kf_1/kf_2, for thick (2.576 mm entry thickness) and thin (0.236 mm entry thickness) gauge rolling passes with three different materials

Material		kf_1 (kN/mm^2)	kf_2 (kN/mm^2)	kf_{eq} (kN/mm^2)	kf_1/kf_2
SS 301	Thick	20.27	70.14	15.72	0.29
	Thin	2051.64	72.18	69.72	28.43
Al 6061-O	Thick	10.10	65.65	8.75	0.15
	Thin	176.01	57.82	43.52	3.04
Cu	Thick	6.76	63.31	6.11	0.11
	Thin	174.58	57.78	43.41	3.02

which is why high-fidelity transfer effects can still be readily seen. Based on this reasoning, however, for Al 6061 and Cu, the transferred high-fidelity deviations should be greater for the thick gauges than for thin gauges, but Fig. 5b seems to contradict this. Ref. [18] also indicates that roughness transfer is expected to be higher in thinner material. However, there cannot be a direct comparison between thick gauge results and thin gauge results here since the total rolling force as well as reduction are different (e.g., 7.495% reduction for thick gauge vs. 1.075% for thin gauge). Also, the results in Figs. 4 and 5 are normalized by input (entry) thickness. Absolute values of the transfer deviations for the thin gauge materials may actually be lower (e.g., 1.47×10^{-3} mm for thin gauge Cu vs. 5.0×10^{-3} mm for thick gauge Cu). Yet, when normalized, the values may be larger (e.g., at location "p" in Fig. 5a and b, the normalized values are 6.21×10^{-3} for thin gauge Cu and 1.94×10^{-3} for thick gauge Cu). While absolute values represent the geometrical error in terms of deviation amplitudes, larger normalized values imply more significant localized flatness defects on the strip due to the relatively greater longitudinal (rolling direction) strains arising from conservation of mass flow during plastic deformation.

Considering the above, a more consequential metric in analyzing transfer effects on the strip geometric quality is the deviation in reduction ratio at a given location compared to the average reduction ratio. This metric is more suitable since it implies related consequences that can lead to the complex flatness defects discussed earlier.

Table 6 RMS error values for exit profile reduction deviation with "warm" work-roll profile in Fig. 1c compared to smooth work-roll, and considering nominal rolling pass parameters in Table 2

Material	Thick gauge	Thin gauge
SS 301	3.03×10^{-4}	1.76×10^{-4}
Al 6061-O	3.33×10^{-4}	1.12×10^{-3}
Cu	3.44×10^{-4}	1.13×10^{-3}

Equations (11) to (13) show the calculation of the deviation in reduction ratio (thickness strain), $\Delta r_e(x)$, at transverse locations x along the exit strip profile, typically taken as Gauss integration points (5 per element) in the SM-FEM model.

$$\bar{r} = 1/n \sum_{i=1}^{n} \frac{H(x_i) - h(x_i)}{H(x_i)} \tag{11}$$

$$\Delta r(x_i) = \frac{H(x_i) - h(x_i)}{H(x_i)} - \bar{r} \tag{12}$$

$$\Delta r_e(x_i) = \Delta r_{in}(x_i) + \Delta r(x_i) \tag{13}$$

In Eqs. (11) to (13), n is the total number of Gauss points, $\bar{r}$ represents the average reduction ratio, $\Delta r(x)$ is the deviation from the average reduction ratio (referred to as "reduction deviation") for the current pass, and $\Delta r_e(x)$ is the total change in reduction deviation considering the entry condition (prior pass input) as well as the exit condition from the current pass. Figure 5c and d shows the corresponding difference in reduction deviation with the high-fidelity grinding error compared to smooth rolls for thick and thin gauge nominal cases with all three materials. To provide a single aggregate "error" transfer metric, a root mean square (RMS) error is calculated via Eq. (14) for n Gauss points based on total reduction deviation considering the roll grinding error (denoted $\Delta r_{e,e}$), as well as total reduction deviation with perfectly smooth rolls (denoted $\Delta r_{e,s}$). Table 6 lists the RMS error in reduction deviation for the nominal cases to be used as a benchmark for parametric studies to analyze the effects of work roll diameter, reduction ratio, and strip width in later sections.

$$RMS = \left[\frac{1}{n} \sum_{i=1}^{n} \left[\Delta r_{e,s}(x_i) - \Delta r_{e,e}(x_i) \right]^2 \right]^{0.5} \tag{14}$$

2.2 Influence of work roll diameter on high-fidelity transfer characteristics

In this section, a case study involving varying the ratio of work-roll diameter to fixed work-roll face length (d_{wr}/l_{wr}) relative to the nominal ratio of 0.25 is carried out to investigate the influence of work roll diameter on the high-fidelity transfer characteristics. The work-roll diameter is thus changed to vary d_{wr}/l_{wr} while maintaining the roll face length and all other parameters (except rolling force) at their nominal values. The required rolling force is re-computed for each diameter, and the transfer of high-fidelity roll grinding deviations is examined to deduce the influence of increasing/decreasing diameter. In doing so, work roll grinding deviations are kept constant, i.e., the absolute roll diameter deviations are directly

Table 7 Normalized specific rolling force values for 7.495% reduction of the thick gauge (2.576 mm)

Normalized diameter	Normalized force ($\frac{Pc}{Ew} \times 10^4$)		
	SS 301	Al 6061-O	Cu
0.167	0.36	0.18	0.12
0.208	0.41	0.20	0.14
0.250	0.45	0.22	0.15
0.292	0.49	0.24	0.16
0.333	0.53	0.26	0.17
0.375	0.57	0.28	0.19

superposed onto the various diameters. Such an approach is deemed more realistic in terms of residual errors in the grinding process, and it provides for direct results comparison. Transfer characteristics are quantified relative to smooth rolls via the RMS error defined in Eq. (14).

As an intermediate calculation, listed in Table 7 are the normalized rolling force values (F_{norm}) required for the thick gauges with each material to achieve the nominal 7.495% reduction. It is evident that with an increase in the work roll diameter, the force required to attain the nominal reduction increases. Increasing the roll diameter results in increased roll-bite contact area, which leads to lower contact pressure, thus to achieve the same reduction larger force is generally required. However, this depends on the specific material properties of the work roll and strip, as well as the updated geometry, as evident in Table 7. Note that required rolling force increases much more rapidly for SS 301 than for Al 6061 and Cu.

Figure 6a and b shows the corresponding kf_1/kf_2 ratios and RMS error values, respectively. Since kf_1/kf_2 is a stiffness ratio, one can intuitively observe the strip exhibits greater "apparent" strength when rolled with larger diameter. Looking at the RMS error, in the case of SS 301, the RMS error continuously decreases with increase in work roll diameter, which is also quite intuitive since the corresponding kf_1/kf_2 ratio increases, implying that the strip behaves stiffer mechanically compared to the work roll as the diameter increases. However, in case of Cu, and up to a certain extent with Al 6061, the RMS error for diameters below nominal reveals a different trend. For cases where work roll diameter is larger than the nominal, the results for all the three materials are consistent, while for lower diameter values, the Cu and Al 6061 first result in increased, but then decreased, RMS errors. The authors believe that the reason such behavior is attributed to the specific rolling force values; when the force is lower for softer materials, the RMS error increases with increase in diameter until reaching a maximum followed by decreasing trend. Four additional d_{wr}/l_{wr} cases ratios between the values of 0.21 and 0.25 are considered to investigate this phenomenon further. It is observed that cases with d_{wr}/l_{wr} less than 0.2375 in both the cases showed increase in RMS error with increasing roll diameter. However, beyond d_{wr}/l_{wr} ratios of 0.2375, all the other cases revealed decreasing RMS errors with increase in roll diameter. Overall, an inverse relationship is revealed between the high-fidelity transfer, based on RMS error, and the stiffness ratio between the strip and work roll, kf_1/kf_2.

In the case of thin gauge passes shown in Fig. 7 (see again Table 2 for gauge and reduction values), strain hardening effects on the strip due to prior reduction can be seen in the required rolling force values listed in Table 8. For the same reduction, rolling force increases greatly with increasing work-roll diameter for the SS 301 compared to Al 6061 and Cu (a gradient of 2.3 exists in the force/diameter relation for SS 301 vs. 0.15 for Al 6061 and Cu, due to roll flattening effect with SS 301). Also, as observed in the previous section, the results for Al 6061 and Cu overlap due to their similar work-hardened strengths. Result trends for the thin gauge are similar to those of the thick gauge, i.e., the ratio kf_1/kf_2 increases, and the RMS error correspondingly decreases, as the work-roll diameter is increased (Fig. 6a and b). However, with the thin gauge, both Cu and Al 6061 show a similar trend to SS 301 since the force values to achieve the 1.075% reduction are relatively larger. It is also evident that since the kf_1/kf_2 ratio values for the softer Al 6061

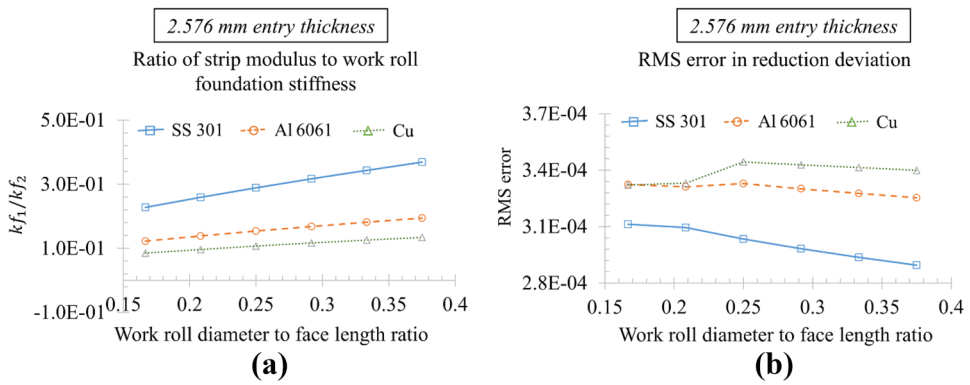

Fig. 6 **a** kf_1/kf_2 ratio and **b** trends in RMS error in reduction deviation as function of work-roll diameter to work-roll face length ratio with the thick gauge (2.576 mm) nominal rolling cases in Table 2, considering three different materials

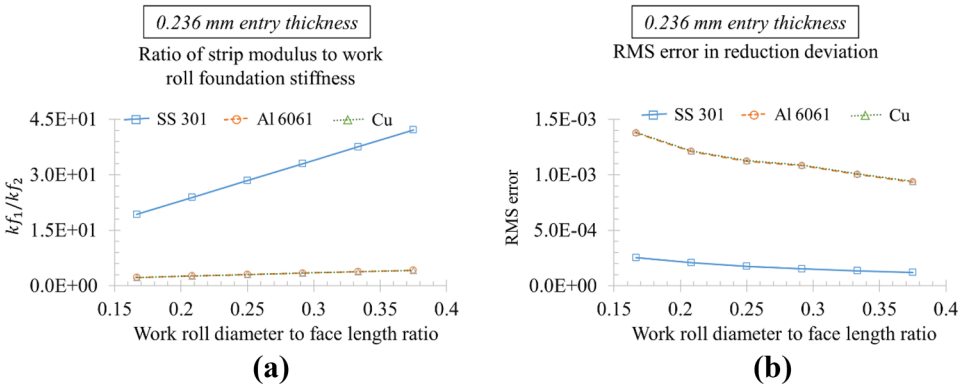

Fig. 7 **a** kf_1/kf_2 ratio and **b** trends in RMS error in reduction deviation as function of work-roll diameter to work-roll face length ratio with the thin gauge (0.236 mm) nominal rolling cases in Table 2, considering three different materials

and Cu materials are lower than for SS 301, they show a more substantial degree of high-fidelity transfer. Note, however, that the rolling force increases relatively linearly with work-roll diameter, the RMS error exhibits a non-linear relation to the ratio d_{wr}/l_{wr}. One reason might be the non-linear nature of rolling force versus mill deflection, which also elucidates the fact that it is not merely the rolling force itself that is responsible for the transfer; i.e., it suggests the presence of the bulk body deformation effects as described earlier.

Interestingly, the results obtained in the above case study involving work-roll diameter effects contradict the conclusions of studies by past researchers in the context of surface roughness or texture transfer [25]. However, it is important to note that there is a perspective difference between the results of past literature and the results here; specifically, in the past studies, conclusions were made regarding the question whether the extent of transfer increases if the roll diameter increases or whether the roughness of the strip is greater when rolled with a larger diameter work roll. The answer might have been concluded as affirmative in an absolute sense, i.e., if the work-roll diameter was increased, the strip might possess greater roughness in experimental tests. However, it is insufficient to conclude that the reason for observed roughness increases was in fact the increase in roll diameter. This is because the approach to conclusion generally did not isolate the influence of work roll diameter itself; indeed, the contact force distribution, and correspondingly the natural crown or thickness profile of the strip, also changes significantly when the roll diameter is changed. In other words, in past studies of roughness and texture, the RMS error or other associated metric used to assess the transfer (e.g., transfer ratio) did not distinguish whether the resulting metric was due to actual transfer mechanism or due in part to bulk body deformation effects that alter the contact force distribution. Moreover, the actual transfer efficiency is likely a combination of both, which can be misleading, as shown in Fig. 8a and b.

To avoid this confounding issue, the RMS error metric in this work reflects the high-fidelity grinding error transfer when benchmarked to the case of perfectly smooth work rolls. Also, the RMS error calculation in this work is based on the values of deviations in the reduction at each point relative to the average reduction of the strip, and not the actual thickness profile. Figure 8 shows the RMS error plot for SS 301 calculated from the exit thickness profile as interpreted in the literature (RMS_{lit}), i.e., with reference to rectangular exit strip profile, as well as with respect to the exit strip when rolled with smooth roll (as in this work, but based on the thickness profile, denoted RMS_t). RMS_{lit} thus represents "absolute" error, while RMS_t represents error relative to otherwise identical smooth (uniform) rolls, as indicated in Eqs. (15) and (16),

$$RMS_{lit} = \left[\frac{1}{n}\sum_{i=1}^{n}\left[\frac{h(x_i)-0}{H(x_i)}\right]^2\right]^{0.5} \tag{15}$$

$$RMS_t = \left[\frac{1}{n}\sum_{i=1}^{n}\left[\frac{h(x_i)_e - h(x_i)_u}{H(x_i)}\right]^2\right]^{0.5} \tag{16}$$

Table 8 Normalized specific rolling force values for 1.075% reduction of the thin gauge (0.236 mm)

Normalized diameter	Normalized force ($\frac{Pc}{Ew} \times 10^4$)		
	SS301	**Al 6061**	**Cu**
0.167	0.41	0.04	0.04
0.208	0.50	0.05	0.04
0.250	0.60	0.05	0.05
0.292	0.70	0.06	0.06
0.333	0.79	0.06	0.06
0.375	0.89	0.07	0.07

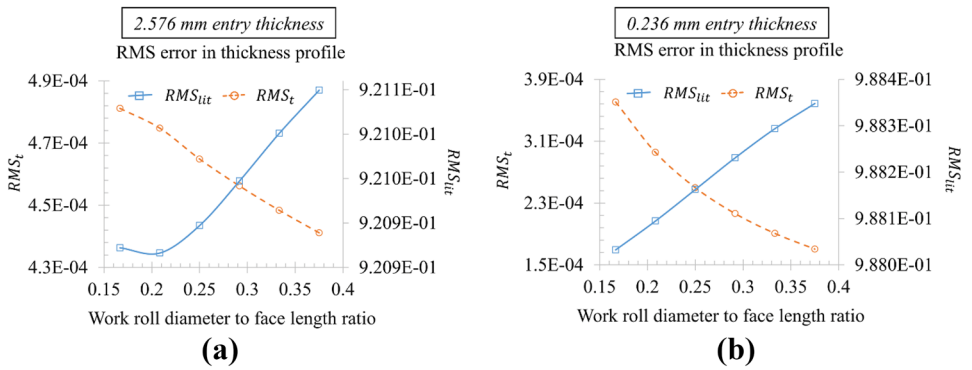

Fig. 8 Absolute RMS error in thickness profile (RMS_{lit}, per Eq. (15)), and RMS error in the relative thickness profile with respect to smooth roll case (RMS_t, per Eq. 16)) to isolate the effects of work roll diameter for SS 301; **a** thick gauge (2.567 mm); **b** thin gauge (0.236 mm)

where $h(x)_e$ and $h(x)_u$ are the exit thicknesses considering grinding error on rolls, and smooth (uniform) rolls, respectively.

From Fig. 8a and b, it can be seen that, with the increase in diameter, error transfer increases in an absolute sense, i.e., if only the final result is considered. However, error transfer is not an isolated effect of the increase in the work roll diameter; a combination of the influence of work roll diameter and contact force distribution (as a result of bulk body deformations that include bending, shear, and variation in Hertzian flattening along the roll face length) produces the results stated in the past literature. Whereas in a truly isolated sense, the influence of work roll diameter is found to be the exact opposite, i.e., with the increase in work roll diameter, the transfer actually decreases. Increasing the work roll diameter changes the contact force and its distribution, so force acting at any particular location "x" may be greater in the case of a larger diameter, and it is this effect that can be dominant rather than the actual influence of the work roll diameter, i.e., compared to when the transfer mechanism is considered fundamentally in terms of its localized contact mechanics. Such a distinction, however, largely depends on the geometry of rolls and the mill configuration and can actually be different for each configuration. A model such as the SM-FEM employed here can thus help provide better clarity in understanding the transfer effects in practical rolling scenarios.

2.3 Influence of reduction ratio on high-fidelity transfer characteristics

A case study with varying the reduction ratio (from the nominal) is carried out to investigate its influence. Recall from Table 2, the nominal reduction ratio is 7.495% for the thick gauge and 1.075% for thin gauge. Exit thickness is varied while maintaining entry thickness and other parameters constant to achieve the different reduction ratios.

The normalized specific rolling force required to achieve the varying reductions based on the thick entry gauge for each material is listed in Table 9. Figure 9a shows the stiffness ratio kf_1/kf_2 for each reduction ratio. It can be noted that the trend between the specific force and kf_1/kf_2 ratio is different from the previous section (influence of d_{wr}/l_{wr} ratio) where both rolling force and kf_1/kf_2 increased in similar fashion. Interestingly, this indicates that even though the rolling force required to achieve the specified reduction increases with increase in the reduction ratio, the effective stiffness ratio, kf_1/kf_2, actually decreases, i.e., the strip "behaves" as softer. This is due to fact that with an increase in reduction ratio, the strip modulus (kf_1) decreases while the elastic foundation of the work roll (kf_2) increases, resulting in a decrease in the ratio overall. One reason behind the decrease in strip modulus is the reduced contribution from elastic recovery. Note also that the plot of kf_1/kf_2 vs. reduction ratio exhibits a non-linear relationship whereby the rate of decrease in kf_1/kf_2 diminishes with an increase in the reduction ratio. This effect can also be seen in the RMS error plot (Fig. 9b). Since the ratio kf_1/kf_2 decreases, it implies the deviations of the work roll penetrate deeper into strip and thus increase the transfer efficiency and in turn the RMS error. It is evident from the kf_1/kf_2 ratio that at greater reduction the work roll behaves relatively stronger against the strip. However, as the reduction ratio increases, or as larger plastic deformation takes place, the strip begins to act with greater apparent strength, thus impeding the transfer efficiency. The actual transfer is, however, a combination of the two counteracting effects,

Table 9 Normalized specific rolling force values for varying reductions of the thick gauge (2.576 mm)

Reduction (%)	Normalized force ($\frac{Pc}{Ew} \times 10^4$)		
	SS 301	Al 6061-O	Cu
3.000	0.36	0.18	0.12
5.000	0.41	0.20	0.14
7.495	0.45	0.22	0.15
11.000	0.49	0.24	0.16
15.000	0.53	0.26	0.17

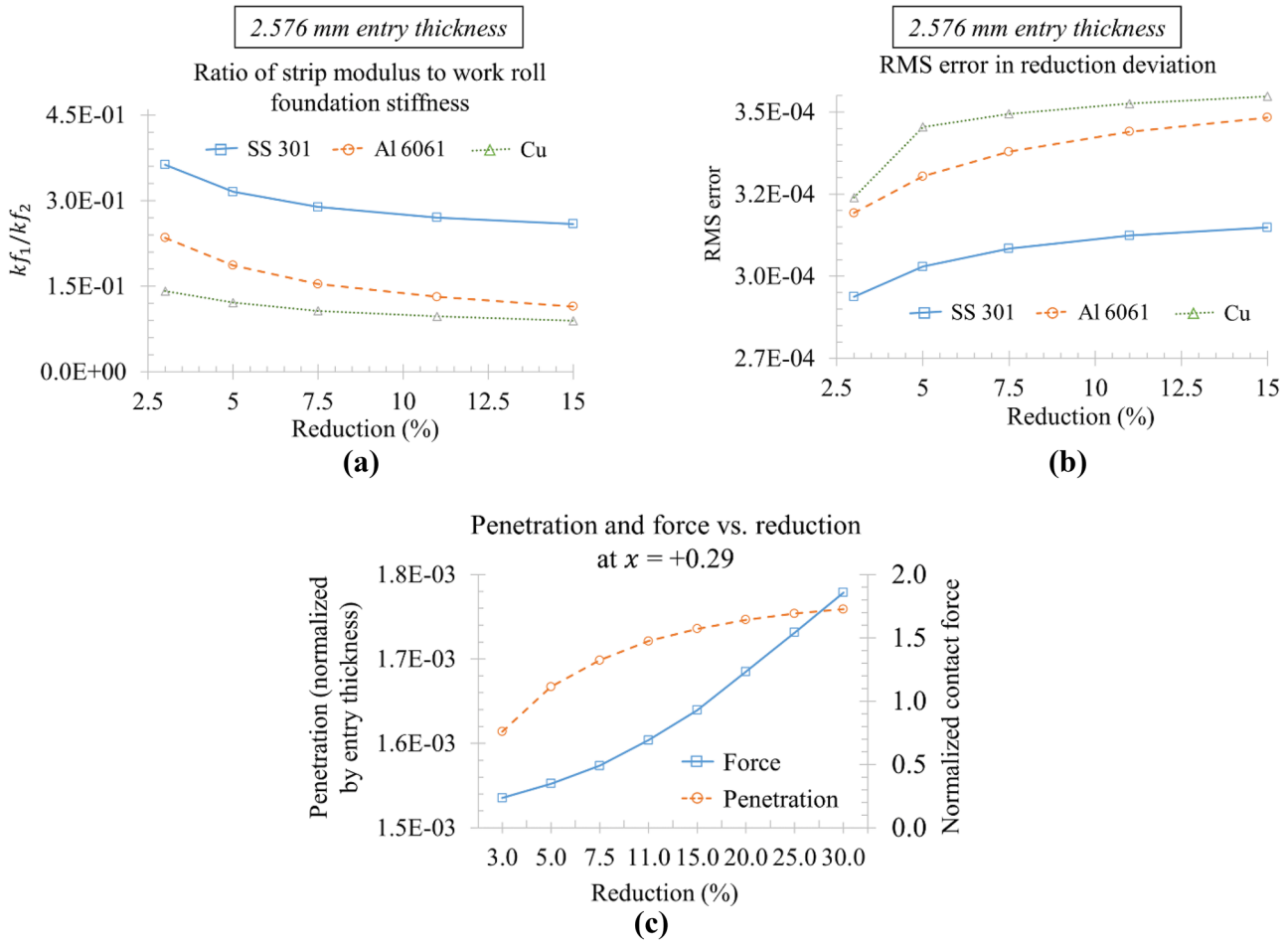

Fig. 9 **a** kf_1/kf_2 ratio and **b** RMS error in reduction deviation at different reduction ratios for thick gauge (2.576 mm); **c** variation of contact force and penetration of work roll deviation into strip at normalized location + 0.29 from mill center for SS 301 thick gauge (2.576 mm) as a function of reduction (%)

which is clearly seen in both the kf_1/kf_2 ratio plot and the RMS error plot. With an increase in reduction ratio, the RMS error does increase; however, the rate of increase diminishes as strain-hardening effects from large plastic deformation begin to dominate the combined effects.

Comparing the three materials, the SS 301 and Al 6061 show similar shapes in the RMS error plots, while for Cu, RMS errors increase abruptly at 5% reduction; thereafter, the change is relatively insignificant. Since Cu experiences the most change in the kf_1/kf_2 ratio at this point, the effect is directly reflected on the RMS error values, while at reduction values beyond this Cu experiences relatively less change in kf_1/kf_2.

It is also intuitive to reason that the increased RMS error seen here is due to the increased force experienced by the high-fidelity roll diameter deviations; that is, with a larger force, work roll geometry peaks penetrate deeper into the strip surface, as has been indicated in past literature. However, this relationship is also complex. For example, Fig. 9c shows the relationship between the contact force at the interface on a particular deviation versus the error (penetration) in the thickness profile of the strip produced by that deviation (the deviation is located at normalized axial distance + 0.29 from the mill center). It is evident from Fig. 9c that with an increase in reduction ratio, even though the force on the deviation at the interface increases, the error in exit strip profile created by that deviation increases nonlinearly and with diminishing rate of increase.

For the thin gauge cases (Fig. 10), the results are similar to those of the thick gauges. Table 10 lists the normalized specific rolling force values needed to achieve the specified reductions. However, a slightly more linear relationship between reduction ratio and RMS error is seen in the thin gauge case. If one briefly re-examines the thick gauge results in Fig. 9b, specifically the cases at lower reduction ratios (less than 5%), a similar linear trend to that of the thin gauge is observed. These results parallel observations made by investigators in [3]. In their analysis, it was observed that

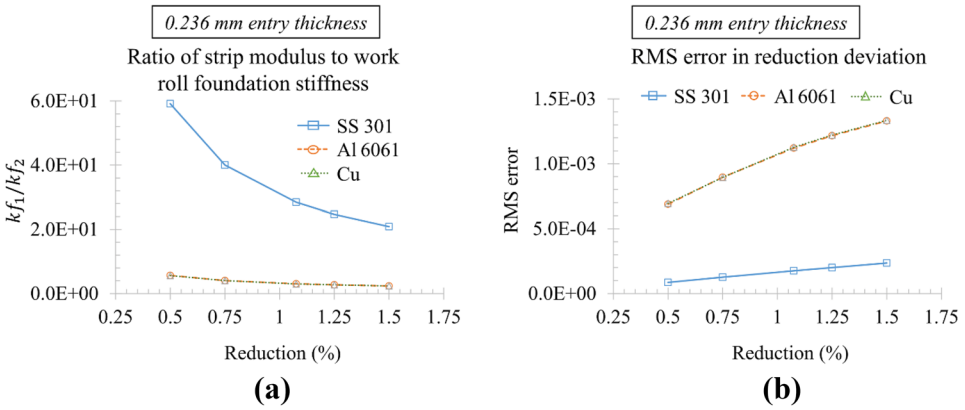

Fig. 10 **a** kf_1/kf_2 ratio and **b** RMS error in reduction deviation for different reduction ratios for thin gauge (0.236 mm)

for a reduction ratio of less than 0.7%, the texture transfer ratio had a linear relationship with the reduction ratio. It is also worth noting that, while the thin gauge Al 6061 and Cu here show the expected trend that is similar to that of the thick gauge, in the case of SS 301, there is a significant drop in the kf_1/kf_2 ratio for the thin gauge case as the reduction ratio increases, even though the force values (Table 10) do not increase considerably. This is due to the fact that in case of SS 301 both the strip and the work roll are composed of same material. However, there is significant work-hardening in the strip due to prior reduction, while work roll still exhibits its original (elastic) mechanical properties, i.e., the effective stiffnesses during rolling are still different between the elastic–plastic strip and elastic work roll. This is also seen in the RMS error plots where SS 301 experiences the least change in transfer behavior among the three materials.

2.4 Influence of strip width on high-fidelity transfer characteristics

A case study with varying the ratio of strip width to roll face length (w/l_{wr}) is conducted to investigate the influence of strip width (roll face length is fixed) on the high-fidelity transfer. Unlike the earlier case studies involving work roll diameter and reduction ratio, the influence of strip width is more challenging to quantify and make reasonable conclusions from the observations due to the complexity in isolating the transfer effects. This is because the fixed positions of high-fidelity deviations along the work roll face make the parametric study difficult since varying the strip width changes the contact length; thus, a wider strip is exposed to larger number of (and different) high-fidelity deviations than a narrow strip, which confounds the comparison of transfer effects.

Table 10 Force values for specified reduction of the thin gauge (0.236 mm)

Reduction (%)	Normalized force ($\frac{Pc}{Ew} \times 10^4$)		
	SS 301	Al 6061-O	Cu
0.500	0.41	0.04	0.04
0.750	0.50	0.05	0.04
1.075	0.60	0.05	0.05
1.250	0.70	0.06	0.06
1.500	0.79	0.06	0.06

A reasonable approach to quantify and compare the transfer effects is to calculate the RMS error in reduction deviation on the strip over a portion of the contact length that is common to all widths considered. Note that changes in the contact force distribution that particular roll diameter deviations are subjected to still occur for the different strip widths irrespective of any contact region examined. Two complicating phenomena worth mentioning, however, are (1) correlation between roll diameter deviations, wherein the influences of high-fidelity deviations at spatially different points have recently been shown to be coupled [33]; and (2) roll diameter deviations at locations that are not actually in the roll/strip contact region also influence the high-fidelity transfer due to bulk body deformation [33]. For instance, given the two different work roll profiles shown in Fig. 11, although identical within the roll/strip contact region, they result in a different exit thickness profiles characterized by RMS error of 3.03×10^{-4} for Profile 1 vs. 3.61^{-4} for Profile 2 (18.62% difference) based on thick gauge Cu rolled with nominal parameters in Table 2.

Despite the foregoing challenges, RMS error calculated with consideration of a common contact length can still provide insights regarding trends in high-fidelity transfer, including due to contact force and distribution changes with varying strip width. Figure 12a shows results for the thick gauge cases for an examined contact region spanning a normalized work-roll face length of − 0.53 to + 0.53. Note that the influence of strip width is similar for all the three materials. The relationship between w/l_{wr} and the RMS error in reduction deviation is almost linear, but the gradient increases beyond a normalized strip width, w/l_{wr}, of 0.6875, or when the strip width is

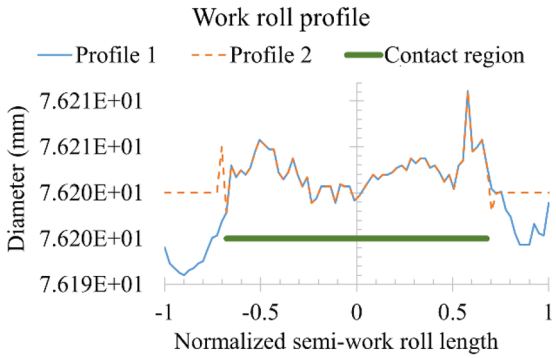

Fig. 11 Different work roll profiles with identical contact region

about 2/3 the roll face length. This case study indicates that wider strip induces greater high-fidelity transfer than narrower strip even when the examined contact region is identical for the RMS error calculation. In the thin gauge cases (Fig. 12b), a similar trend is observed, again with increase in the gradient of RMS error for w/l_{wr} exceeding 0.6875. As was seen in the previous case studies, the significantly work-hardened thin-gauge SS 301 strip exhibits much lower high-fidelity transfer compared to the Al 6061 and Cu.

The reason for different gradients either side of $w/l_{wr} = 0.6875$ lies in the natural deformation behavior of the mill and the accompanying contact force distribution, which ultimately leads to well-known "natural crowning" of the strip (in the absence of any corrective crown control mechanisms). Figure 13a shows the natural crown for the different strip widths on the 4-high mill under consideration. It is evident that the nominal strip width corresponds approximately to the maximum relative crown (crown as ratio of entry thickness), while the other width cases produce smaller relative crowns. To more closely identify the normalized width at which the peak natural crown occurs, three more cases for w/l_{wr} in the range 0.6875 to 0.7708 are examined (Fig. 13b). The maximum is subsequently observed for w/l_{wr} of about 0.72 to 0.73. For further insight into the influence of strip width on the high-fidelity transfer, another case study involving only a single deviation (corresponding to the maximum deviation on the warm diameter work roll profile in Fig. 1c) present at different locations on the work roll face length was carried out for the thick-gauge SS 301. Results from this study help reveal not only the relationship between the contact force and the high-fidelity transfer, but also the "efficiency" of transfer at different roll face-length locations.

Figure 14a shows the RMS error for cases in which the location of a single (maximum) deviation is varied across the work-roll face length. Since, under ideal conditions with uniform rolls, the strip thickness would be symmetric about the mill center, nine cases for locations varying from the left strip edge to the mill center are assessed. Also, since the single deviation will not only induce transfers at its own location but rather along the entire strip width, due to correlation effects (but which are usually greater in the vicinity of roll deviation vicinity), the same RMS error metric is used for quantitative analysis. The plot in Fig. 14a shows that, although the single roll profile deviation is identical, its location has a significant impact on the extent of transfer. This difference stems from the bulk-body mill deformation. To eliminate the effect of the different roll/strip contact force at the different locations, Fig. 14b provides the corresponding RMS error when calculated from ratio of normalized error to normalized contact force at each Gauss point in the SM-FEM model, i.e., at each Gauss point, the effect on the strip thickness profile is normalized in addition to normalizing the corresponding contact force at that point so that a non-dimensional value is obtained that represents the transfer effect per unit normalized contact force. It can be seen in Fig. 14b that, with such analysis, the location of the deviation in fact influences the transfer amount. It is worth noting here that this type of analysis is only possible with a 3D roll stack model; a plane strain model or other simplified models cannot reveal such effects. Considering the results in Fig. 14b, one may intuitively reason that the absence of a crown control mechanism such as work roll bending, which

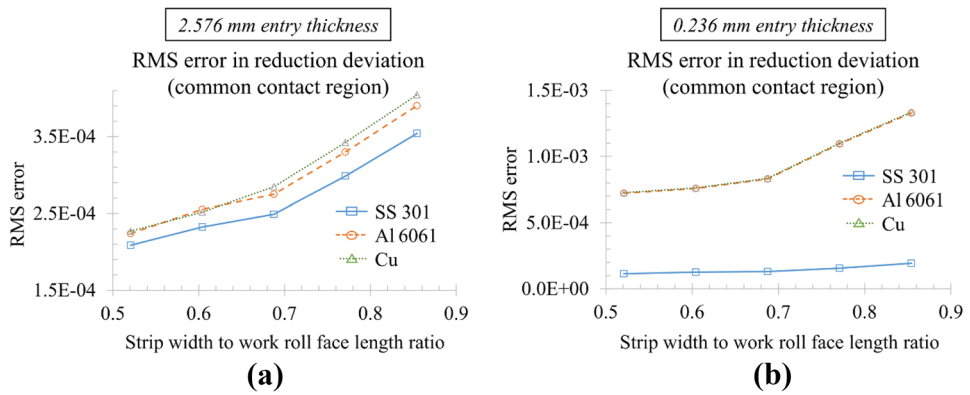

Fig. 12 RMS error in reduction deviation for different ratios of strip width to work-roll face length: **a** thick gauge (2.576 mm); **b** thin gauge (0.236 mm)

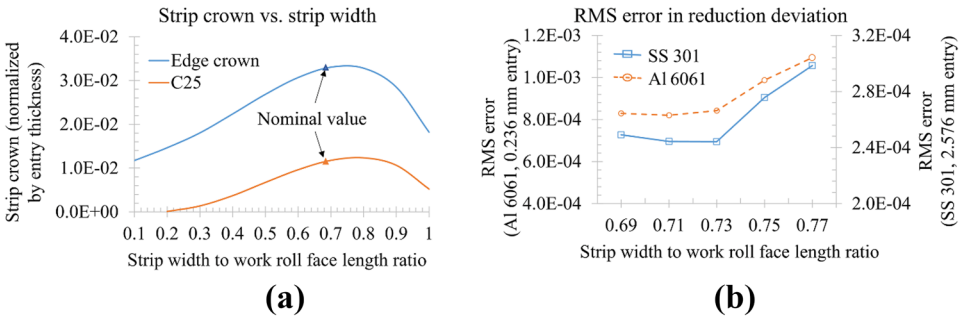

Fig. 13 **a** Natural crown of strip versus strip width to work roll face length ratio; **b** RMS error in reduction deviation for w/l_{wr} ratio between 0.6875 and 0.7708

results in the large natural strip crown, is in fact the cause of such behavior. However, as is discussed in the next section, work roll bending has no effect on the RMS error in Fig. 14 (see Fig. 15c and d).

3 Work roll bending as corrective mechanism

Although it is widely accepted in practice that work roll bending and other conventional flatness control mechanisms are not designed to address localized variations in thickness strain, the case studies in this section aim to clearly demonstrate this inability based on the high-fidelity roll grinding error represented in Fig. 1c. The parametric work roll bending studies in this section assume that the incoming strip inherits the thickness profile and mechanical properties based on output from prior rolling passes according to the nominal case parameters in Table 2 (e.g., Fig. 4a, b). Also, for the work roll bending analyses, all rolls (including the upper work roll) are now assumed to be perfectly smooth. Fundamentally, work-roll bending acts as a "low-frequency filter" for adjusting the strip profile and corresponding flatness; and, as will be shown, the previous transfer from such high-fidelity roll grinding defects discussed in this work remains virtually unaffected by work-roll bending effects.

Figure 15a shows the combined reduction deviation (reduction deviation of the incoming strip plus reduction deviation induced by the current pass) for the thick gauge SS 301 with different amounts of work-roll bending. Since the incoming strip thickness profile is convex overall due to the natural crown, the outgoing strip in this case also exhibits a crown since the current reduction is more uniform due to the inclusion of work roll bending effects (Fig. 15b). However, the high-fidelity deviations from the roll grinding error transfer are not readily seen on the reduction deviation output in Fig. 15a. Note also that the height of the deviation peaks is attenuated in the current pass. References [19, 30, 44, 45] show similarly that roughness of the strip decreases after a rolling pass employing smooth rolls. From Fig. 15b, it is evident that the reduction in the current pass is in fact not "smooth"; high-fidelity deviations in the current pass reduction are clearly seen. Now, if the relative difference is considered between the incoming high-fidelity thickness profile (i.e., with roll grinding error) and an incoming ideal thickness profile (i.e., no grinding error), as shown in (Fig. 15c), then it is clear that the high-fidelity remains unaffected by work-roll bending. Indeed, Fig. 15c demonstrates that high-fidelity deviations are unaffected at every value of work-roll bending applied since the relative difference plot is indistinguishable; and the RMS errors obtained are thus the same for the different values of work-roll bending (Fig. 15d). The thick gauge Al 6061 (Fig. 16) and Cu (Fig. 17) materials exhibit similar results to the SS 301, but since Al 6061 and Cu are much softer than the work-roll compared to SS 301, the extent of attenuation for Al 6061 and Cu is far greater than for SS 301. Even though the attenuation for SS 301 here is lower, the fact that the height of high-fidelity peaks on the incoming strip profile is less is the reason for the apparent lower deviation in the current pass.

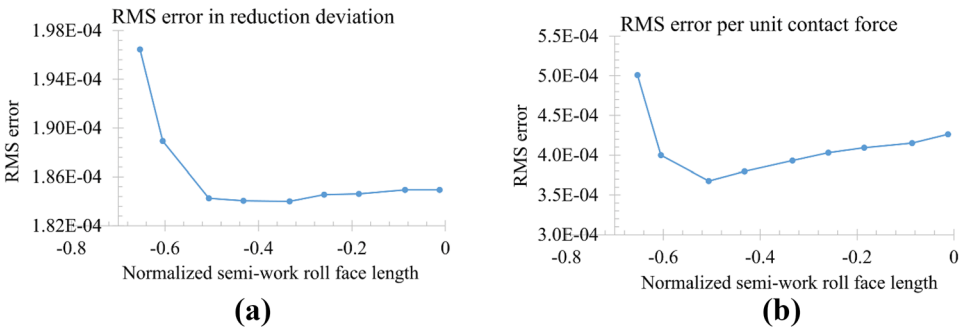

Fig. 14 **a** RMS error in reduction deviation for a single deviation at different locations; **b** corresponding RMS value per unit normalized rolling force

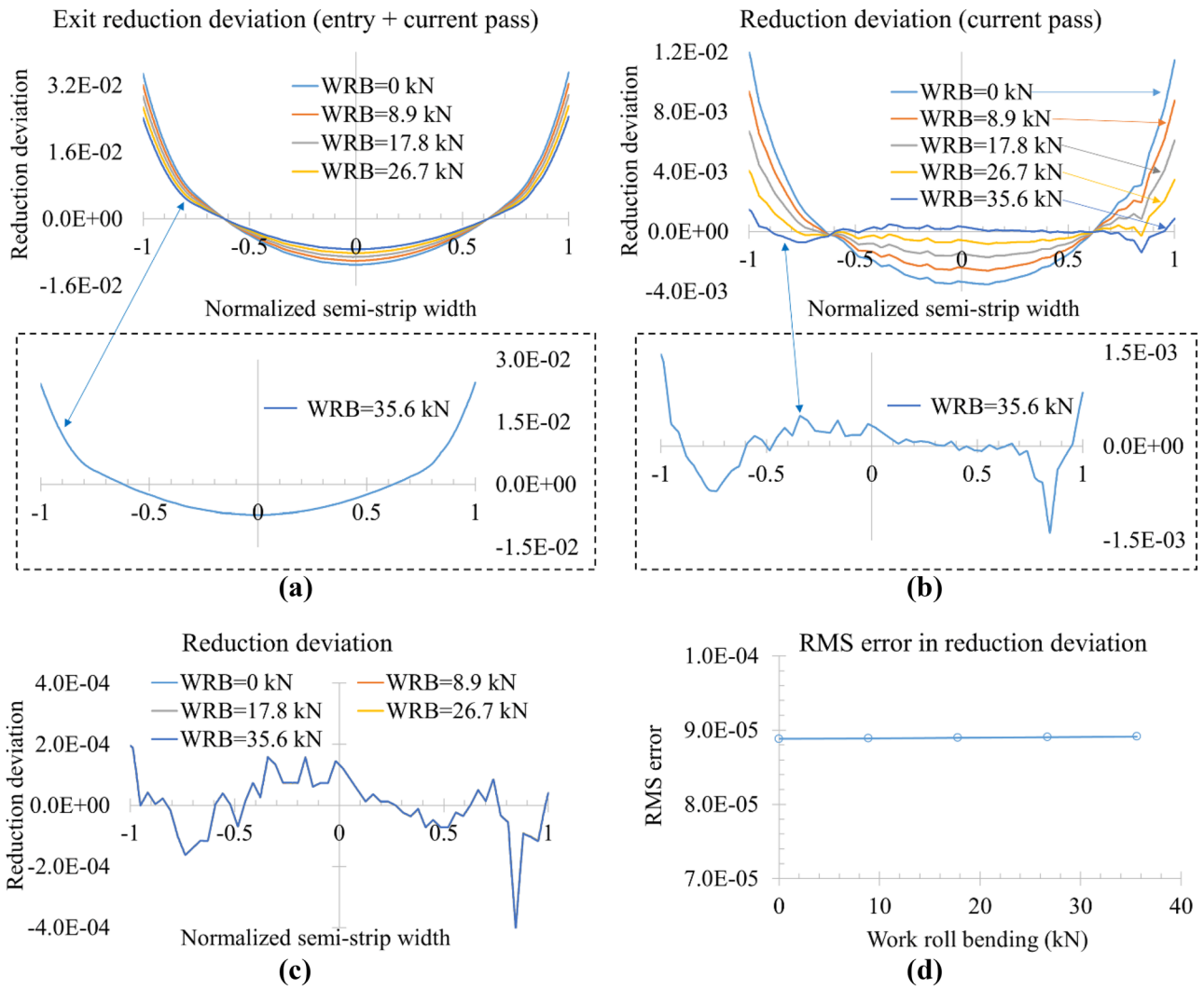

Fig. 15 **a** Total reduction deviation (entry + exit); **b** reduction deviation induced in the current pass for SS 301 thick gauge; **c** relative difference in the reduction deviation of entry strip (from prior pass with roll grinding error) compared to ideal entry strip; **d** RMS error in reduction deviation for current pass considering various amounts of work-roll bending (WRB)

Similar to the foregoing results for thick gauges, the thin gauge SS 301 and Al 6061 cases are shown in Figs. 18 and 19, respectively. In the thin gauge cases, the high-fidelity transfer for Al 6061 and Cu (where Cu exhibits similar results to Al 6061 due to comparable strengths following work hardening) can be easily seen. For SS 301, however, the plots of reduction deviation are fairly smooth (both consider the current pass only with incoming deviations). The smoothness of the reduction deviation of the current pass implies it to be essentially a scaled profile of the incoming

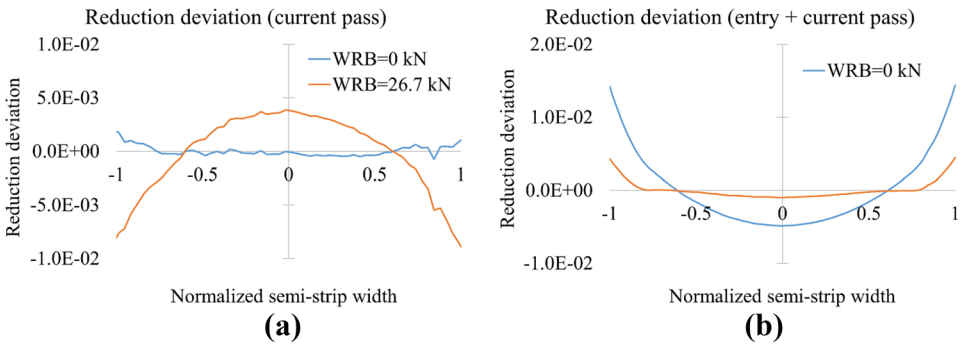

Fig. 16 **a** Reduction deviation induced in the current pass and **b** total reduction deviation of Al 6061-O thick gauge (2.576 mm)

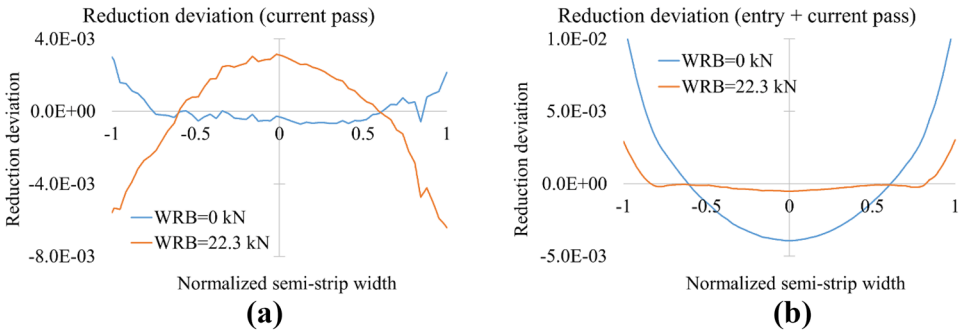

Fig. 17 **a** Reduction deviation induced in the current pass and **b** total reduction deviation of Cu thick gauge (2.576 mm)

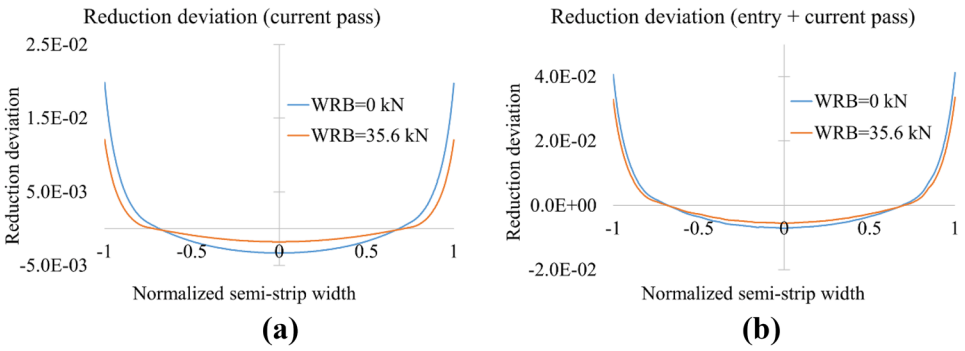

Fig. 18 **a** Reduction deviation induced in the current pass and **b** total reduction deviation of SS 301 thin gauge (0.236 mm)

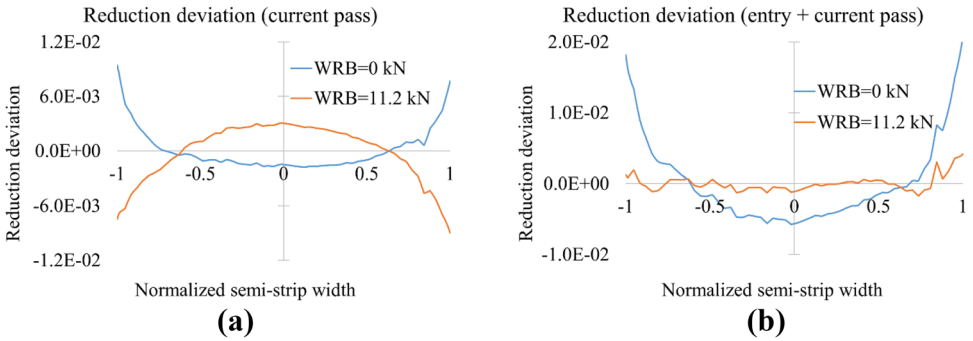

Fig. 19 **a** Reduction deviation induced in the current pass and **b** total reduction deviation of Al 6061-O thin gauge (0.236 mm)

strip; hence, there is no considerable thickness variation locally. Although the incoming strip contained very small high-fidelity roll grinding error transfer, the outgoing strip in this case has the negligible high-fidelity thickness deviations simply because the incoming deviations were negligible.

4 Corrective work-roll grinding

In the studies presented to this point, the degree of transfer from high-fidelity work roll grinding errors on to strip has been parametrically examined, and the prior section confirmed that work roll bending cannot remove high-fidelity thickness profile defects arising from the roll grinding error. The focus is now turned to a new way of addressing such high-fidelity deviations using a "corrective" work-roll grinding approach, which at some point could be implemented in situ[3] in a closed-loop flatness control system. The high-fidelity thickness profiles characterized earlier in Fig. 4a and b are now considered as incoming strip for a subsequent rolling pass in which the effectiveness of "engineered" corrective roll grinding profiles are investigated as to their capability to significantly eliminate the high-fidelity strip thickness profile deviations. Corrective grinding profiles are imposed only on the upper work roll. Incoming strip without previous high-fidelity thickness profile deviations are also simulated here assuming perfectly smooth rolls in order to obtain a reference profile for effective comparison. Considering the possibility of

[3] An effective and adequate debris removal system would be required.

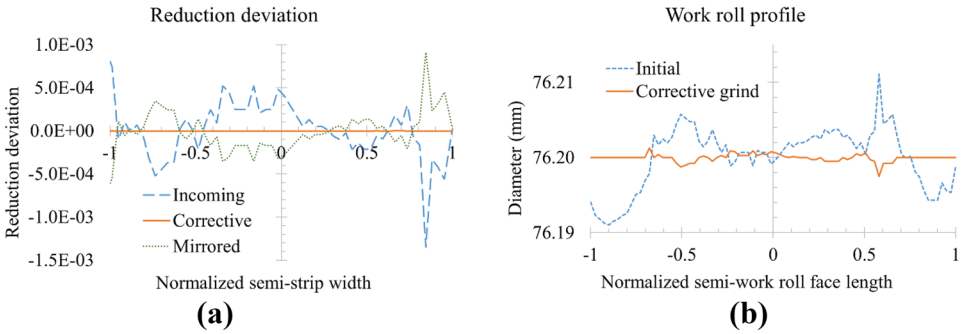

Fig. 20 **a** Reduction deviation and **b** corrective work-roll grinding pattern for SS 301 thick gauge (2.576 mm)

corrective work roll grinding profiles, the presence of bulk body deformations such as bending, shear, and variations in Hertzian roll flattening, together with recently reported micro-to-macro scale coupling effects [33], necessitates the need to "engineer" the corrective grinding patterns rather than to simply apply scaled "mirror" image patterns of the defects.

Indeed, a 3D model such as the SM-FEM formulation used in this work is prerequisite since 2D plane strain and otherwise simplified models lacking transverse behavior do not account for the 3D bulk body deformation. Moreover, contact force distributions are different for a strip rolled with a work roll containing high-fidelity deviations versus that with a smooth roll; and this phenomenon cannot be predicted by 2D models or models lacking sufficient transverse fidelity. One aspect of particular difficulty in designing a corrective roll grind profile is the correlation among spatially separated diameter deviations along the roll axis. The difficulty arises because the influence of transfer at one transverse (roll axis) location on the roll/strip interface affects the influence at all other locations on the interface. Hence, in the design of a corrective work-roll grinding pattern, points on the roll profile cannot be determined independently. The significance of this is that corrective grinding can also not be achieved by merely correcting for specific, individual deviations. Earlier it was even shown (Fig. 11) that details of work-roll profile at axial locations not in the strip contact region also influence the resulting contact force and exit thickness profile. With a corrective grinding profile applied to strip having high-fidelity defects, the correlation is more complicated since neither opposing surface has low-order surface geometry variation (i.e., neither is smooth). In this preliminary work, corrective work-roll grinding profiles are engineered by trial-and-error using the SM-FEM model, and the performance of these is compared to roll profiles based on "mirror images" of the high-fidelity strip profile defects imparted during the previous pass. The purpose is to highlight points made in the above discussion.

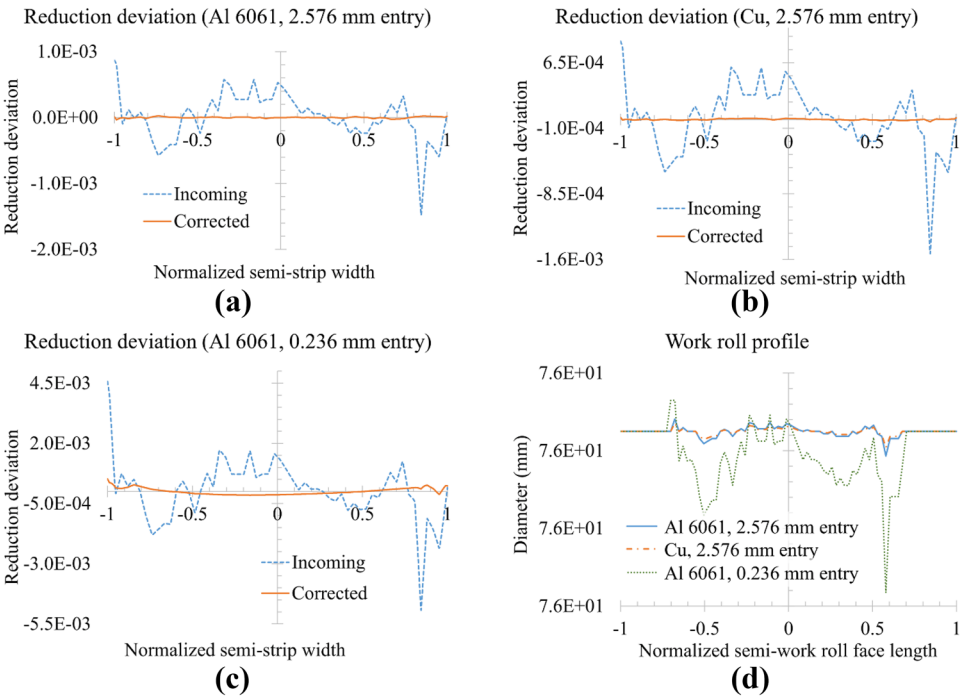

Fig. 21 Incoming and corrected reduction deviation for **a** Al 6061-O thick gauge (2.576 mm); **b** Cu thick gauge (2.576 mm); **c** Al 6061-O thin gauge (0.236 mm), and **d** corrective grind for work roll

Figure 20a shows the outgoing (exit gauge) reduction deviation from a SS 301 rolling pass with the same nominal parameters in Table 2 (except for thickness and corresponding force changes) based on a "trial-and-error" corrective work-roll grinding pattern and a mirror image pattern according to the incoming strip profile reduction deviation from the prior pass. In Fig. 20b, the corrective grinding pattern resembles a reduced scale mirror image of the initial warm work-roll profile (in Fig. 1c), but it is in fact an adjusted profile that also accounts for the effects of non-uniform deflections of rolling mill and its components.

Figure 21 shows the incoming and outgoing (exit gauge) reduction deviations and the corresponding corrective work-roll grinding Cu (thin gauge Al 6061 results are similar). Note that even though the incoming profile looks similar in each case (Fig. 21a, b, and c), the scales and range of the plots are different. The amplitudes of the deviations in the incoming profile in each case are different; thus, to correct for them adjustments have to be engineered according to the specific deviations and material properties (e.g., roll/strip stiffness ratio), particularly since the natural mill deflection behaviors are unique and lead to different corrective grinding patterns (Fig. 21d). Table 11 lists the RMS error relative to that with perfectly smooth work rolls for both the incoming and outgoing strip condition.

Even though the corrective roll grinding approach described here is a successfully demonstrated and novel concept, it presents a large number of technical challenges in terms of in situ practical application. For instance, grinding tools and machines for such high-precision grinding may render this approach infeasible at present. Even with such capability, the transient nature of work roll profile (for instance thermal expansions, wear) and of incoming strip profile requires such tools to be used online, which poses another dimension of challenges such as debris management, lubrication management, dynamic nature of mill, dynamic nature of the grinding operation itself, and their associated effects and influence on the strip evolution.

Table 11 RMS error in reduction deviation for passes with corrective work-roll grinding

Case	RMS error	
	Incoming	Output
SS301 thick	3.03×10^{-4}	1.46×10^{-5}
Al 6061-O thick	3.33×10^{-4}	1.00×10^{-5}
Cu thick	3.44×10^{-4}	7.36×10^{-6}
Al 6061-O thin	1.12×10^{-3}	1.30×10^{-4}

5 Conclusions

A comprehensive study of the transfer behavior of high-fidelity deviations from the work roll on the strip in a 4-high mill has been carried out using root-mean-square (RMS) error in reduction deviation (with reference to smooth uniform roll case) as a metric to investigate the influence of rolling parameters such as work roll diameter, reduction ratio, strip width, and strip material strength. Application of the results from the detailed parametric studies is leveraged to provide fundamental insights into novel corrective work-roll grinding profiles that are shown to significantly reduce high-fidelity thickness profile defects from the rolled strip. In contrast to similar studies on the parametric influences of roughness in the field of texture transfer, the presented work illustrates the importance of effective isolation of the variables and consideration of bulk body deformations such as bending, shear, and flattening in the transfer. This work also illustrates the capability of the 3D roll-stack SM-FEM model to effectively and efficiently predict the effects of high-fidelity contact surface deviations and interactions where coupling effects exist between the micro- and macro-scale deformations under diverse varying conditions. Case studies carried out with an efficient 3D roll-stack model formulated using the SM-FEM method culminate in the major findings listed below:

Bulk-body deformations can significantly strengthen or attenuate the high-fidelity deviations transfer. In the theoretical absence of bulk-body effects, the transfer mechanism is governed mainly by ratio of the elastic foundation stiffness of the strip (kf_1) to the elastic foundation stiffness of the work roll (kf_2).

The relationship between work-roll diameter and high-fidelity deviation transfer is found to be inversely proportional in general. The RMS error in reduction deviation decreases with an increase in work-roll diameter under the same rolling conditions. However, in case of softer materials, the RMS error increases initially up to work roll to diameter ratio of 0.2375.

High-fidelity deviation transfer increases with an increase in reduction ratio; however, the relationship is fairly non-linear. The rate of increase in RMS error diminishes with an increase in reduction ratio due to strain hardening effects from large plastic deformation and the elastic recovery of the strip.

RMS error increases with wider strips; however, the results can be inconclusive since the reason for higher transfer might not be solely due to change in strip width. The ratio of strip width to roll face length inherently changes the natural crown of the strip, which can play a similar role to bulk-body deformation.

The thickness profile error produced on the strip by transfer of the high-fidelity work-roll deviations depends

not only on the deviation height and loading condition but also significantly on the transverse location of the particular deviation along the roll face length, due to non-negligible bulk-body deformation.

Because of the highly localized nature of the high-fidelity defects, work roll bending is ineffective as a correction mechanism. While the amplitude/height of peaks on the strip diminishes in a subsequent pass using perfectly smooth work rolls, the valleys remain unaffected.

Due to the presence of bulk-body deformation such as bending, shear, and varying Hertzian flattening, the correction of such high-fidelity deviations on the strip cannot be made using a simple (scaled) mirror image of the incoming deviations.

Author contribution Patel, A.: Conceptualization, methodology, formal analysis, investigation, data curation, writing, and visualization. Malik, A.: Conceptualization, methodology, software, resources, data curation, writing, supervision, project administration, and funding acquisition. Zhang, F.: Software. Mathews, R.: Formal analysis, writing, and visualization.

Funding This research was funded by National Science Foundation, grant number CMMI-1555531.

Availability of data and material Available upon request.

Code availability Available upon request.

Declarations

Ethics approval Not applicable.

Consent to participate Not applicable.

Consent for publication The authors give their consent for publication.

Conflict of interest The authors declare no competing interests.

References

1. Patel A, Malik A, Mathews R (2022) Efficient three-dimensional model to predict time history of structural dynamics in cold rolling mills. J Manuf Sci Eng 144:071009. https://doi.org/10.1115/1.4052703
2. Brewster DB (1989) Profile control by distributed control systems : dream or reality? Tappi journal (USA)
3. Wu C, Zhang L, Qu P, Li S, Jiang Z (2018) A simple approach for analysing the surface texture transfer in cold rolling of metal strips. Int J Adv Manuf Technol 95:597–608. https://doi.org/10.1007/s00170-017-1218-9
4. Lechler Inc Precision nozzles and systems for roll cooling solutions in rolling mills
5. Tlusty J, Chandra G, Critchley S, Paton D (1982) Chatter in cold rolling. CIRP Ann 31:195–199
6. Yun I-S, Wilson WRD, Ehmann KF (1998) Chatter in the strip rolling process, part 1: dynamic model of rolling. J Manuf Sci Eng 120:330–336. https://doi.org/10.1115/1.2830131
7. Hu P-H, Ehmann KF (2000) A dynamic model of the rolling process. Part I: homogeneous model. Int J Mach Tools Manuf 40:1–19. https://doi.org/10.1016/S0890-6955(99)00049-8
8. Hu P-H, Ehmann KF (2000) A dynamic model of the rolling process. Part II: inhomogeneous model. Int J Mach Tools Manuf 40:21–31. https://doi.org/10.1016/S0890-6955(99)00050-4
9. Zhao H (2008) Regenerative chatter in cold rolling. Ph.D. Dissertation, Northwestern University
10. Yun I-S, Ehmann KF, Wilson WRD (1998) Chatter in the strip rolling process, part 2: dynamic rolling experiments. J Manuf Sci Eng 120:337–342. https://doi.org/10.1115/1.2830132
11. Yun I-S, Ehmann KF, Wilson WRD (1998) Chatter in the strip rolling process, part 3: chatter model. J Manuf Sci Eng 120:343–348. https://doi.org/10.1115/1.2830133
12. Hu P-H, Zhao H, Ehmann KF (2006) Third-octave-mode chatter in rolling. Part 1: chatter model. Proceedings of the Institution of Mechanical Engineers, Part B: Journal of Engineering Manufacture 220:1267–1277. https://doi.org/10.1243/09544054B06804
13. Hu P-H, Zhao H, Ehmann KF (2006) Third-octave-mode chatter in rolling. Part 2: stability of a single-stand mill. Proceedings of the Institution of Mechanical Engineers, Part B: Journal of Engineering Manufacture 220:1279–1292. https://doi.org/10.1243/09544054B06904
14. Hu P-H, Zhao H, Ehmann KF (2006) Third-octave-mode chatter in rolling. Part 3: stability of a multi-stand mill. Proceedings of the Institution of Mechanical Engineers, Part B: Journal of Engineering Manufacture 220:1293–1303. https://doi.org/10.1243/09544054B07004
15. Gao Z-Y, Liu Y, Zhang Q-D, Liao M-L, Tian B (2020) Chatter model with structure-process-control coupled and stability analyses in the cold rolling system. Mech Syst Signal Process 140:106692. https://doi.org/10.1016/j.ymssp.2020.106692
16. Özakın B, Çolak B, Kurgan N (2021) Effect of material thickness and reduction ratio on roughness transfer in skin-pass rolling to DC04 grade sheet materials. ILT 73:676–682. https://doi.org/10.1108/ILT-10-2020-0377
17. Wu C, Zhang L, Qu P, Li S, Jiang Z (2019) A new method for predicting the three-dimensional surface texture transfer in the skin pass rolling of metal strips. Wear 426–427:1246–1264. https://doi.org/10.1016/j.wear.2018.12.020
18. Çolak B, Kurgan N (2018) An experimental investigation into roughness transfer in skin-pass rolling of steel strips. Int J Adv Manuf Technol 96:3321–3330. https://doi.org/10.1007/s00170-018-1691-9
19. Xia C, Zhang X, Zhang J, Li H, Jia S (2017) Evolution on topography of textured work rolls and steel strips during cold rolling and temper rolling. steel research int 88:1600469. https://doi.org/10.1002/srin.201600469
20. Wentink DJ, Matthews D, Appelman NM, Toose EM (2015) A generic model for surface texture development, wear and roughness transfer in skin pass rolling. Wear 328–329:167–176. https://doi.org/10.1016/j.wear.2015.02.015
21. Kijima H (2013) Influence of roll radius on contact condition and material deformation in skin-pass rolling of steel strip. J Mater Process Technol 213:1764–1771. https://doi.org/10.1016/j.jmatprotec.2013.04.011
22. Kijima H (2014) Influence of roll radius on roughness transfer in skin-pass rolling of steel strip. J Mater Process Technol 214:1111–1119. https://doi.org/10.1016/j.jmatprotec.2013.12.019
23. Li C, Fu B, Zhu T, Li Y (2014) Roughness and glossiness of SUS430 stainless steel in cold rolling. Procedia Engineering 81:167–172. https://doi.org/10.1016/j.proeng.2014.09.145
24. Belov VK, Begletsov DO, D'yakova MV, Gorbunov AV, (2014) Production of sheet with regulated surface microtopography. Steel Transl 44:298–305. https://doi.org/10.3103/S0967091214040020
25. Kimura Y, Ueno M, Mihara Y (2009) Printing behavior of roll surface texture to hot-dip galvanized steel sheet in temper rolling. Tetsu-to-Hagane 399–405

26. Kijima H, Bay N (2008) Skin-pass rolling I—studies on roughness transfer and elongation under pure normal loading. Int J Mach Tools Manuf 48:1313–1317. https://doi.org/10.1016/j.ijmachtools.2008.06.005
27. Kijima H, Bay N (2008) Skin-pass rolling II—Studies of roughness transfer under combined normal and tangential loading. Int J Mach Tools Manuf 48:1308–1312. https://doi.org/10.1016/j.ijmachtools.2008.06.006
28. Tieu AK, Liu YJ (2004) Friction variation in the cold-rolling process. Tribol Int 37:177–183. https://doi.org/10.1016/S0301-679X(03)00048-3
29. Ma B, Tieu AK, Lu C, Jiang Z (2002) An experimental investigation of steel surface characteristic transfer by cold rolling. J Mater Process Technol 125–126:657–663. https://doi.org/10.1016/S0924-0136(02)00377-1
30. Le HR, Sutcliffe MPF (2000) Analysis of surface roughness of cold-rolled aluminium foil. Wear 244:71–78. https://doi.org/10.1016/S0043-1648(00)00441-5
31. Bünten R, Steinhoff K, Rasp W, Kopp R, Pawelski O (1996) Development of a FEM-model for the simulation of the transfer of surface structure in cold-rolling processes. J Mater Process Technol 60:369–376. https://doi.org/10.1016/0924-0136(96)02356-4
32. Plouraboué F, Boehm M (1999) Multi-scale roughness transfer in cold metal rolling. Tribol Int 32:45–57. https://doi.org/10.1016/S0301-679X(99)00013-4
33. Zhang F, Malik AS (2021) An efficient multi-scale modeling method that reveals coupled effects between surface roughness and roll-stack deformation in cold sheet rolling. J Manuf Sci Eng. https://doi.org/10.1115/1.4050714
34. Zhang F, Malik AS, Yu H (2018) High-fidelity roll profile contact modeling by simplified mixed finite element method. In: Volume 4: Processes. American Society of Mechanical Engineers, College Station, Texas, USA, p V004T03A034
35. Malik AS, Grandhi RV (2008) A computational method to predict strip profile in rolling mills. J Mater Process Technol 206:263–274. https://doi.org/10.1016/j.jmatprotec.2007.12.026
36. Park H, Hwang S (2017) 3-D coupled analysis of deformation of the strip and rolls in flat rolling by FEM. steel research int 88:1700227. https://doi.org/10.1002/srin.201700227
37. Xie L, He A, Liu C (2018) A rapid calculation method for predicting roll deformation of six-high rolling mill. J Iron Steel Res Int 25:901–909. https://doi.org/10.1007/s42243-018-0131-2
38. Guo R-M, Malik AS (2005) Development of a new crown/shape control model for cluster mills. Iron and Steel Technology 2:31–40
39. Malik AS, Hinton JL (2012) Displacement of multiple, coupled Timoshenko beams in discontinuous nonlinear elastic contact, with application to rolling mills. J Manuf Sci Eng 134:051009. https://doi.org/10.1115/1.4007185
40. Zhang F, Malik A (2018) A roll-stack contact mechanics model to predict strip profile in rolling mills with asymmetric, continuously variable crown rolls. J Manuf Sci Eng 140:011008. https://doi.org/10.1115/1.4037600
41. Matsubara S, Hara K, Takezoe A (1989) Optimization of work roll taper for extremely-thin strip rolling. ISIJ Int 29:58–63. https://doi.org/10.2355/isijinternational.29.58
42. Nelson AW, Malik AS, Wendel JC, Zipf ME (2014) Probabilistic force prediction in cold sheet rolling by Bayesian inference. J Manuf Sci Eng 136:041006. https://doi.org/10.1115/1.4027434
43. Lenard JG (2004) The effect of roll roughness on the rolling parameters during cold rolling of an aluminum alloy. J Mater Process Technol 152:144–153. https://doi.org/10.1016/j.jmatprotec.2004.03.026
44. Jiang ZY, Zhu HT, Tieu AK (2006) Mechanics of roll edge contact in cold rolling of thin strip. Int J Mech Sci 48:697–706. https://doi.org/10.1016/j.ijmecsci.2006.01.017
45. Jiang ZY, Tieu AK (2007) Contact mechanics and work roll wear in cold rolling of thin strip. Wear 263:1447–1453. https://doi.org/10.1016/j.wear.2006.12.068